Research report no. 3

# Innovative Solutions for Air Distribution in Vehicles Cabin

# PhD Supervisors:

Assoc. Prof. PhD. Eng. IlincaNastase in coutelle with

Prof. PhD. Eng. Amina Meslem

PhD Student: Eng. Paul Danca

# Contents

I.	Introduction3	
II.	Purpose of this study5	
1.	Study realisation necessities	6
1.1.	Thermal environment evaluation	7
	► Particle Image Velocimetry – PIV	7
	► Laser Doppler Velocimetry - LDV	9
	► Hot wire anemometry	. 13
	► Other equipments	. 14
1.2.	Thermal comfort evaluation	. 15
	► Other thermal comfort assessment equipamnets	. 15
	► Thermal manikin	. 15
Ш	. Numerical model construction:23	
	► The first step - drawing of the Megane geometry and mashing the calculation volume	. 23
	► The second step is validation of the numerical model	. 23
	► The third step - introduction of a virtual thermal manikin in to the cabin model	. 27
	► The fourth part is presented validation of the numerical model including the manikin	. 29
2.	Numericam model tests	. 48
Bil	bliography55	

## I. Introduction

Thermal comfort in the vehicles cabins were carried out in in the last decades and arestill ongoing due to the complexity of theenvironment, which it make difficult to predict the optimal adjsustments to achieve thermal comfort. On the other hand there is a demand to reduce the energy consumption and in the same time to provide a comfortable thermal environment. The actual standards dedicated to this area, complicates things even more by proposing evaluation models developed and dedicated to the buildings environment, which are not adapted to the transient and non-uniform environment from the vehicles.

Previously, in the first report is presented the heating/cooling systems in the vehicles from the beginning and their evolution over the time; Also, a review of the evaluation models proposed by the standards and other new models developed during the timeare presented along with some literature results. The most important conclusions of this report are that the existent ventilation systems do not provide a thermal comfortable environment for the passengers while thestandardized evaluation models are not adapted to the cabin thermal environment demands.

The second report contains the informations about the experimental evaluation of thermal comfort and indoor air quality in the passenger compartment. The actual standards propose three evaluation models, each of these with a different methodology. Each methodogy is described in the second part while in the first part of the report, are listed the measurement tools we used along with the measurement principles.

In the present report are presented the numerical and experimental studies performed until this moment, a short description of the experimental measurement tools that are used, and the construction of the numerical model. Also numerical simulations and validation of the numerical model can be found in the second part of the report. For a better understanding of actual situation in research field, in the following are resumed the ain ideas of the bibliographic study. The actual studies are divided in two big categories: Numerically and Experimentally. Each of these categories includes three subcategories, presented in Figure 1.

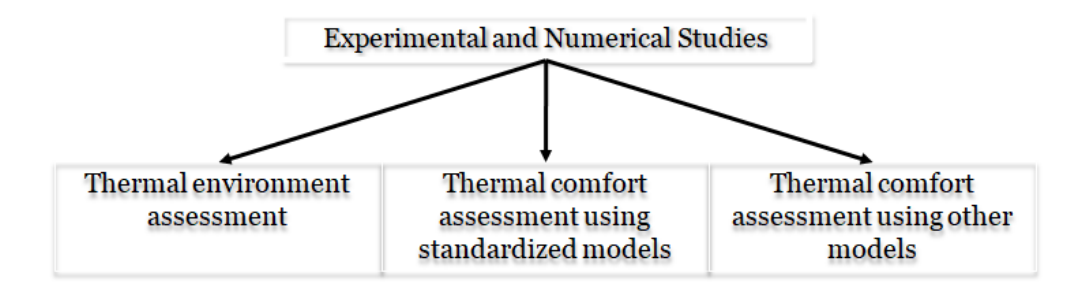


Figure 1. Schematic divirion of the actual studyes

The conclusions of the available experimental studies are:

- Most of the numerical studies are focusing of an accurate prediction of the environmental parameters inside the vehicle. Some of the researchers performed a serious validation of the numerical model
- Some of the studies are focusing on the evolution of these environmental parameters in time as a result of their interdependent variation, the objective being for instance to demonstrate that the climate inside the vehicle might be far from any comfort limit. Studies are focusingmostly on the summer time
- There are some numerical studies in which are used PMV/PPD models and virtual manikins are providing teq.
- Most of the studies omit the consideration of solar radiation.
- Some studies are using the coupling between CFD and thermo-physiological nodal models. This strategy is allowing to impose dynamic boundary conditions for the human body and to have in the same time an evaluation of the local thermal sensation. This is the most effective way to simulate transient conditions in a vehicle. However, these models are almost impossible to be validated experimentally.

#### The conclusions of available numerical studies are:

- Most of the numerical studies are focusing of an accurate prediction of the environmental parameters inside the vehicle. Some of the researchers performed a serious validation of the numerical model
- Some of the studies are focusing on the evolution of these environmental parameters in time as a result of their interdependent variation, the objective being for instance to demonstrate that the climate inside the vehicle might be far from any comfort limit. Studies are focusingmostly on the summer time
- There are some numerical studies in which are used PMV/PPD models and virtual manikins providing teq
- Most of the studies omit the consideration of solar radiation
- Some studies are using the coupling between CFD and thermo-physiological nodal models. This strategy is allowing to impose dynamic boundary conditions for the human body and to have in the same time an evaluation of the local thermal sensation. This is the most effective way to simulate transient conditions in a vehicle. However, thesemodels are almost impossible to validate experimentally
- SI CARE E DIFERENTA DINTRE NUMERIC SI EXPERIMENTAL ? PAR LA FEL

## II. Purpose of this study

Considering the main conclusion from the bibliographic study, the purpose of this thesis is to improve thermal state of the passengers of motor vehicles, trough changes madeon the ventilation system. During the PhD. will be studied the effect of different ventilation configuration and blowers geometryes Figure 2 over the cabin thermal environment on a side and on the other hand over thermal comfort. The thermal environment evaluation is often found in the literature because ithelps to understand better the penomenas who occur in cabin. The more complex way to evaluate the thermal confort is in both ways, numerical and experimental.



Figure 2. The geometry of the inlet grills

The realization plan of this studyis as follows:

- the first is will be evaluated experimentally the effects classical ventilation system, provide by the car manufacturer. In the same time the vehicle cabin geometry will be drawn, in catia and then will be inported in design modeler. The very next step is model meshing and the solution independence checking.
- using the datasoptained from the first experimental seson, the cabin numerical model will be validated.
- after the validation of the cabin model, an virtual manikin will be added to it in the place of the driver.
- another experimental measurement session with Suzy thermal manikin will be done in order to validate numerical model including thermal maniki.
- different situation will be simulated using the numerical model with the manikin, including different inlets geometry.

The obtained results will be compared between them and with other resultsfrom literature. Due to the CFD simulation we have posibility to reproduce the same initial

condition, extracting thermal parameters distribution maps, thermal phenomena what will occur in the vehicle compartment will be better understand, while the experimental measurements results are serving as input data for numerical model and especially for validation.

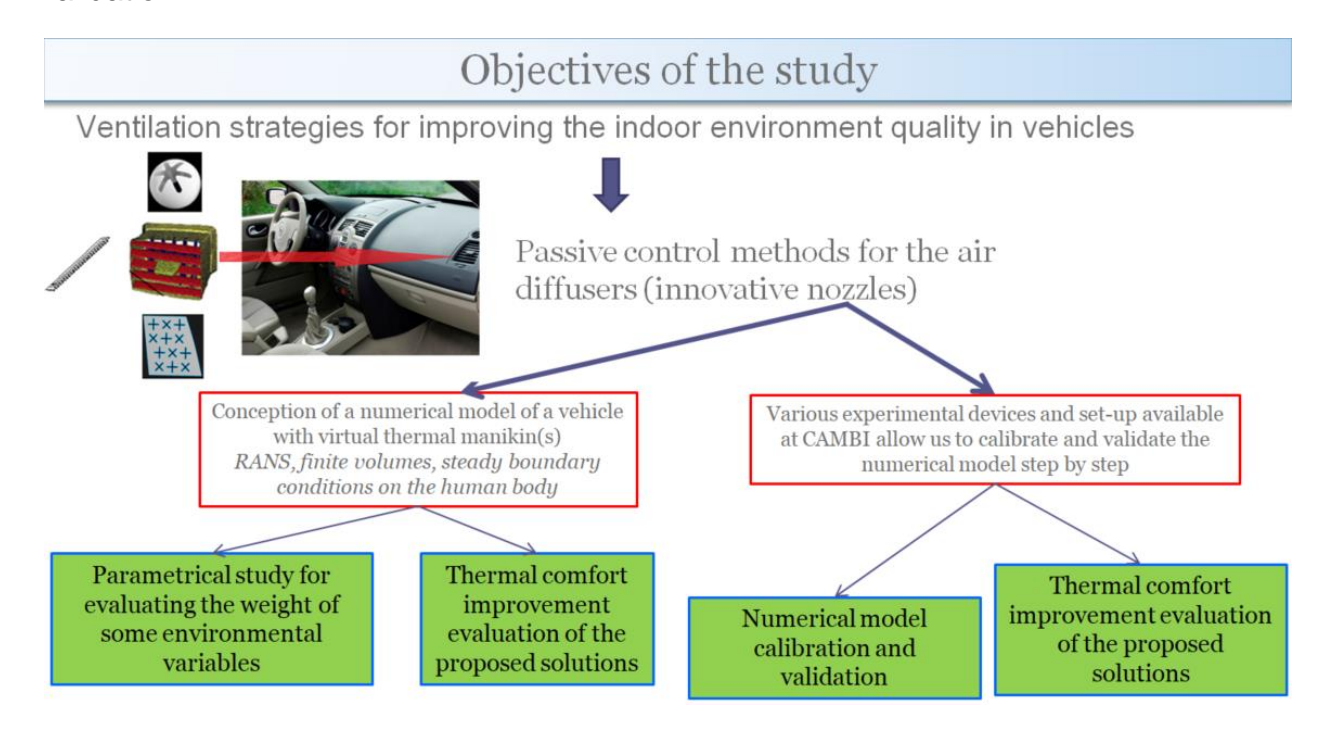


Figure 3. Realisation plane of this study

As is shown in Figure 3, this study is divided in two parts: numerical part and experimental parts. Each of these parts is important in its own way and between them is an indispensable link.

In the first part of the next chapter are sortly presented measurement equipaments, their construction, their operating principle and and their usefulness. In the second part is described the construction steps of the numerical model and its validation.

# 1. Studyrealisation necessities

A Renault Megane hatchback car with a 1.4 liter engine, with a manual ventilation/conditioning system is used for thermal comfort study. The ventilation system has three types of discharge grills: one at the dashboard leveldirected to the windshield; four grilles that are directed to the passengers from the front part of the vehicle and four discharge grills that are directed to the legs of both front and the rear passengers. Because we don't have acces to a climatic chamber big enough to fit the vehicle in order to obtain controlled conditions, for the experimental studies the car was kept inside a hall were indoor conditions varied slower than outside.

#### 1.1. Thermal environmentevaluation

## ► Particle Image Velocimetry – PIV

The PIVmeasurement thehnique found its roots in Laser speckle velocimetry, a technique that several groups began experimenting with in the late 1970s. In the early 1980s it was found that it was advantageous to decrease the particle concentration down to levels where individual particles could be observed. At these particle densities it was further noticed that it was easier to study the flows if they were split into many very small 'interrogation' areas, which could be analyzed individually to generate one velocity for each area. The images were usually recorded using analog cameras and needed immense amount of computing power to be analyzed.

With the increasing power of computers and widespread use of CCD cameras, digital PIV has become increasingly common, to the point that it is the primary technique today.

Particle image velocimetry is an optical method to investigate fluid flow and to measure velocities in a fluid. This is a non-intrusive flow thechnique which allows measuring an entire field of speeds.

At the base of this flow measurement technique is the interrelation of consecutive images of a flow recorded by the CCD or CMOS sensors. Previously in the the fluid is seeded with fine loquid or solid particles. The essential principle of PIV measurement method is the determination of local flow velocities from local particle displacements. In a very short time period  $\Delta t$  (who is known), a particle is moving from the position  $\vec{x}$  to position  $\vec{x} + \vec{\Delta x}$ , the local deplacement velocity can be determinate with the following relation:

$$v(\vec{x},t) = \frac{\overrightarrow{\Delta_x}(\vec{x},t)}{\Delta_t}$$
 (1)

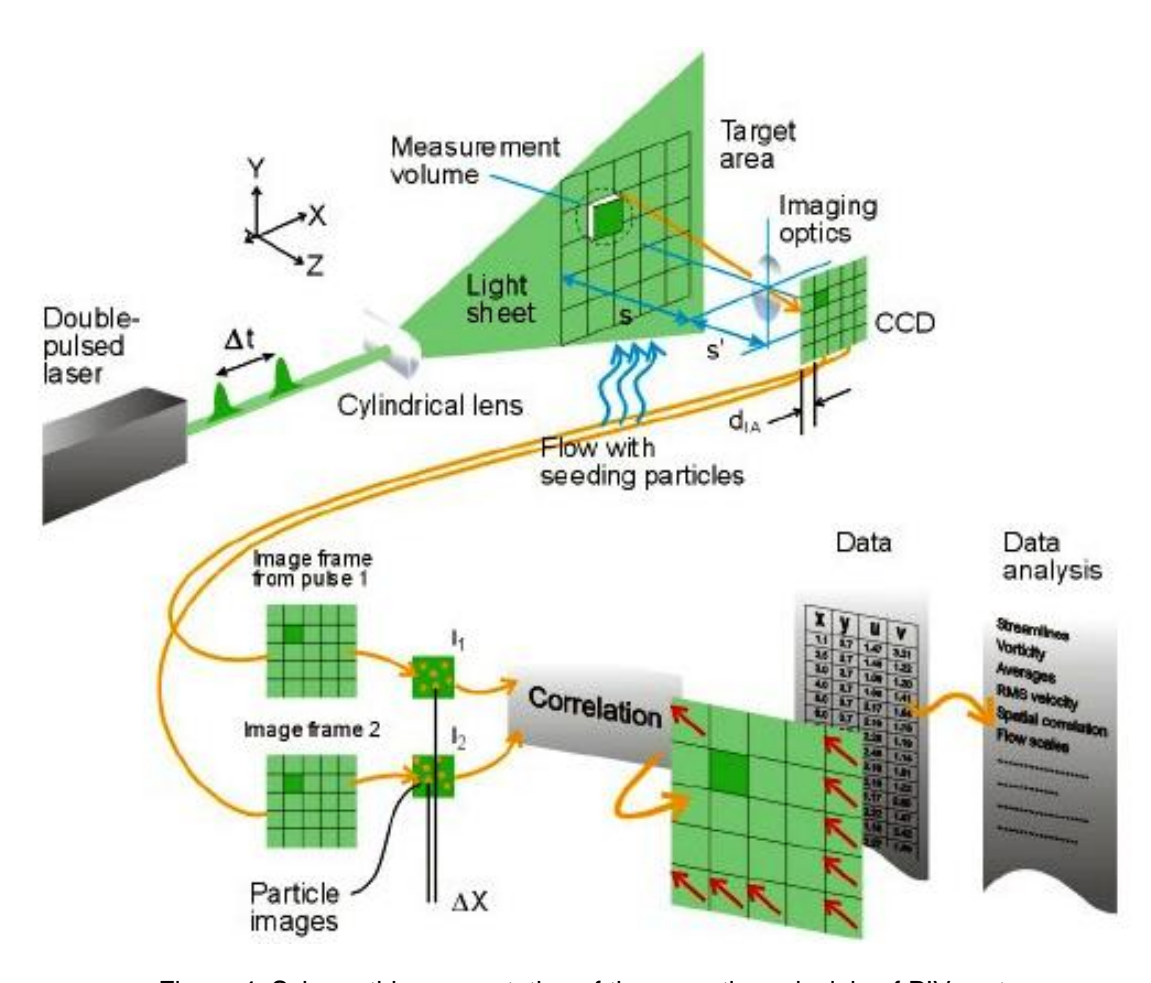


Figure 4. Schemathicpresenatation of the operating principle of PIV system

For this porpouse the broadcast signal of the particles is recorded, on two successive images, separated in time with  $\Delta t$ . Then a spatial intercalation statistical treatment on the numbered images is applied $\hat{l}$ ndepending on their gray level. In order to be able to obtain the local speed vectors, the images are divided into small windows called correlation grid. The velocity field is better solved in space if the correlation grid in finer.

The PIV measurement technique is perfectly suited for viewing instantaneous flow velocity fields. Choosing particle sizes for PIV measurements is often a compromise between the need for a low relaxation time given by a reduced particle size and a sufficient diffusion of light from retro-diffusion lighting orby a high intensity light source. In general, for PIV measurements, controlling the amount of particles introduced into the flow is a delicate phase because in addition to homogeneity of seeding, a particle density of at least 8 must be ensured on each interrogation cell. Another aspect who needs attention is the average number of pixels associated with a particle. Thereby it need to checked if the particle measures around 2 x 2 pixels, after the camera lens and the measuring field are fixed.

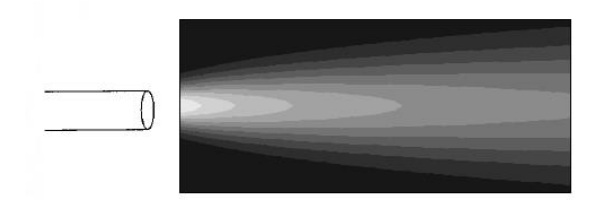
Particle Image Velocimetry (PIV) - instantaneous measurement of 2 components in a plane

conventional methods (HWA, LDV)

- · single-point measurement
- · traversing of flow domain
- time consuming
- only turbulence statistics

particle image velocimetry method

- · whole-field method
- non-intrusive (seeding)
- · instantaneous flow field





The 2D PIV system that is available at UTCB is composed of a high sensitivity camera FlowSense MKII 4M with the resolution of 106 pixels and a Quantel laser of 200mJ. This laser produces a bright plan haveing the wavelength of 532nm. The acquisition frequency of the system is of 7Hz. Image calibration resulted in spatial resolution of 0.3mm/pixel which corresponds to a viewing field of 600mm×600mm.

## ► Laser Doppler Velocimetry - LDV

A Laser Doppler Velocimeter (LDV), also known as a Laser Doppler Anemometer (LDA), is a type of interferometer that measures the velocity of objects using laser light. The objects can be microscopic particles in a fluid or solid surfaces—the concept is even used in some high-end laser mice.

With the development of the helium—neon laser (He-Ne) at the Bell Telephone Laboratories in 1962, the optics community had available a source of continuous wave electromagnetic radiation highly concentrated at a wavelength of 632.8 nanometers (nm), in the red portion of the visible spectrum[4]. It was soon shown fluid flow measurement could be made from the Doppler effect on a He-Ne beam scattered by very small polystyrene spheres entrained in the fluid [5].

At the Research Laboratories of Brown Engineering Company (later Teledyne Brown Engineering), this phenomenon was used in developing the first laser Doppler flowmeter using heterodyne signal processing[6].

The instrument was soon called the laser Doppler velocimeter (LDV) and the technique laser Doppler velocimetry, also abbreviated LDV. Another application name is laser Doppler anemometry (LDA). Early LDV applications ranged from measuring and mapping the exhaust from rocket engines with speeds up to 1000 m/s to determining flow in a near-surface blood artery. A variety of similar instruments were developed for

solid-surface monitoring, with applications ranging from measuring product speeds in production lines of paperand steel mills, to measuring vibration frequency and amplitude of surfaces. [7]In the case of this non-intrusive measurement method no calibration is required, the noise level is very low, the response is high frequency and the speed is measured independently of other variables. One of the advantages of this technique is thet the measurement volume is very small. In the Figure 5 are presented the compenent of the system and in Figure6is represented schematic operating principle of Laser Doppler Anemometer. The laser beam is splitted in two and is focused by a lent, at the intersection of these two beams the probe volum is formed. An interference pattern is generated, and light and dark stripes form inside the probe volume (Figure7). These stripes are called "fringes".

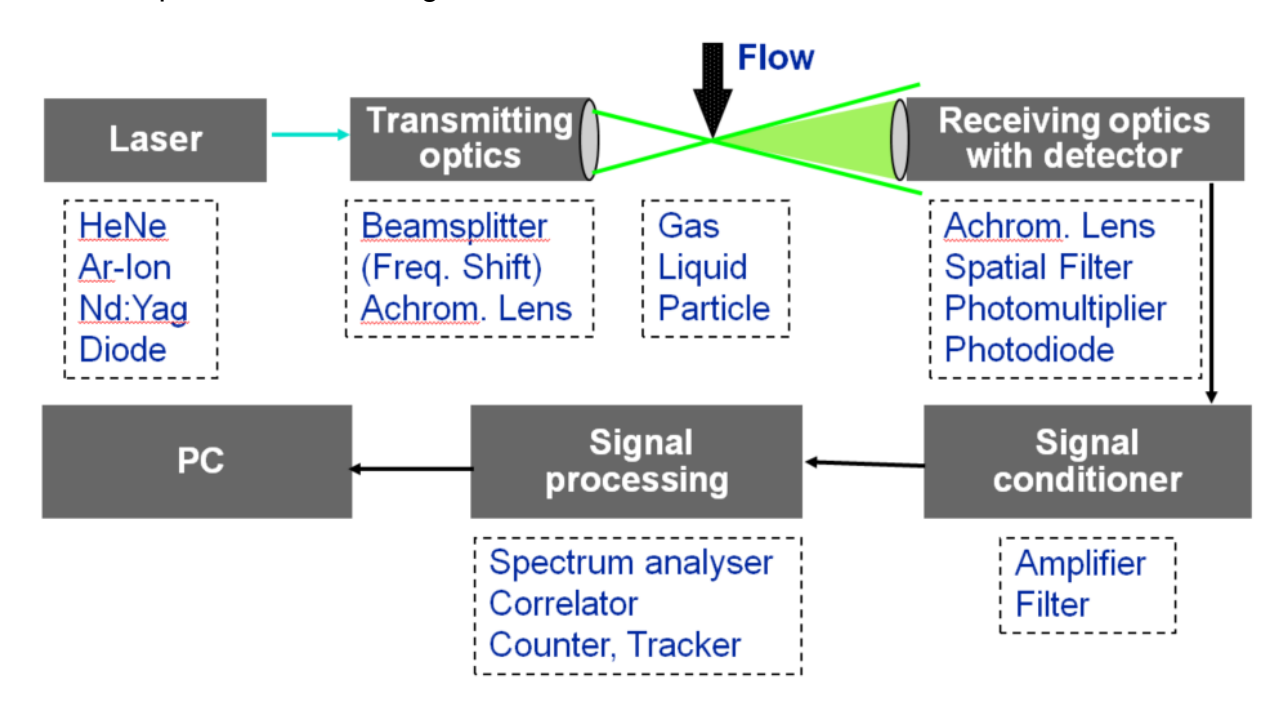


Figure 5 the components of LDV system

The fringes formed by the interference of the beams are a pattern of light in space. When a particle passes through the probe volume, it goes through the light and dark regions, it reflects the light in all directions. A part of this light is retrieved in retro diffusion by a photomultiplier. Its reflected light is measured as it travels along, the intensity versus time curve looks like a sinusoid with a Gaussian envelope.

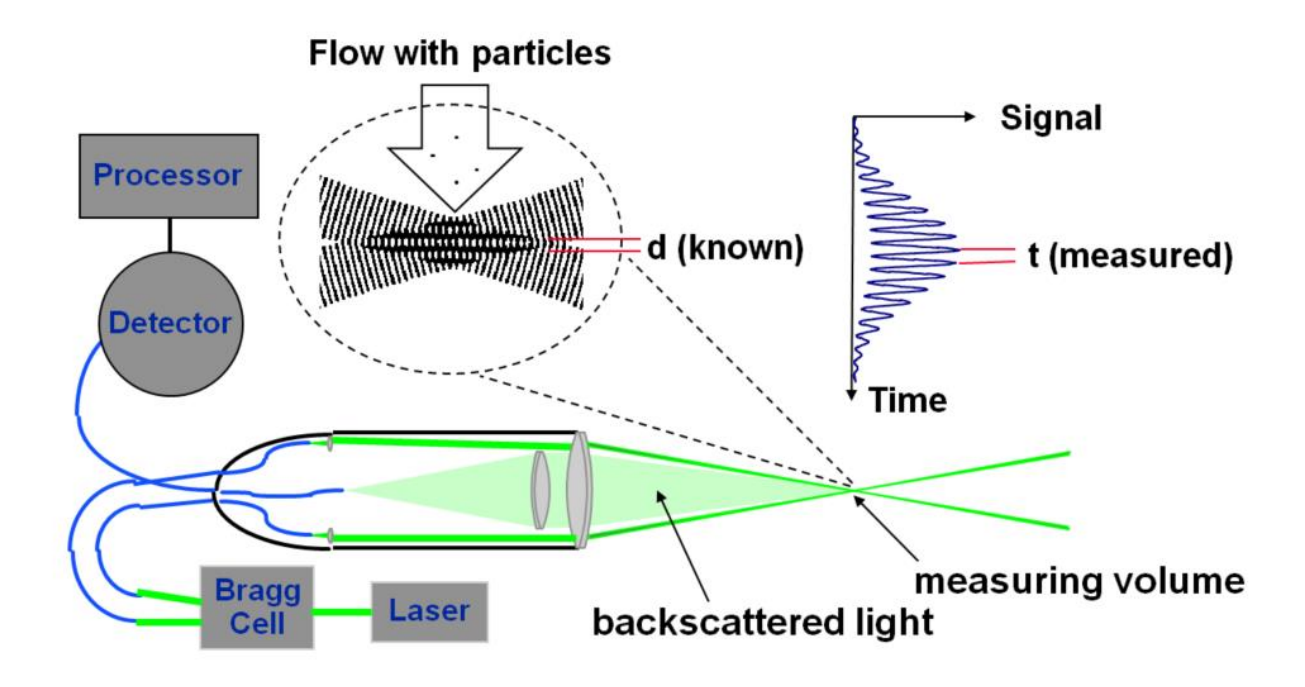


Figure 6. The scheme of operating principle of the system LDV

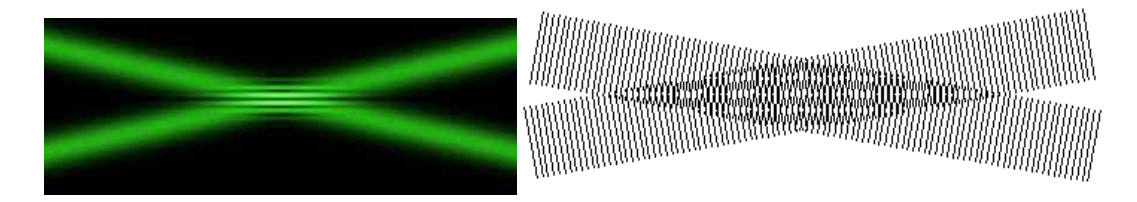


Figure7.Measuring volume

The Gaussian envelope comes from the fact that the intensity of the beams is Gaussian in nature. The sinusoid is the physical travel of the particle through the fringes. The physical distance between the fringes is known from the calibration which is performed with every probe. So the frequency of the intensity signal is directly proportional to the velocity of the particle: velocity = fringe spacing x intensity frequency.

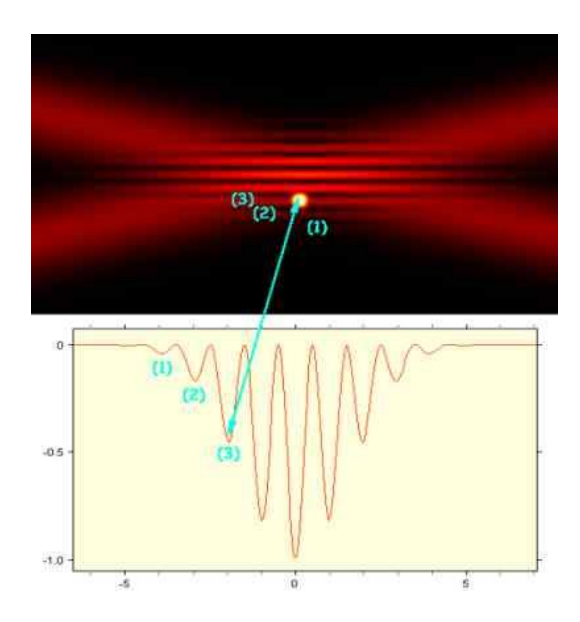


Figure 8. The signal given by the photomultiplier, with the characteristic frequency

In order to achieve accurate measurement, a particular attention should be directed to construction of stripes ("fringes") system in the same time a homogeneous sowingmust to be ensured. For a better system performance the two beams "bragg-at" and "ne-bragg-at" intensity must to be equal and at their intersection a perfect ellipsoid must be created (Figure9).

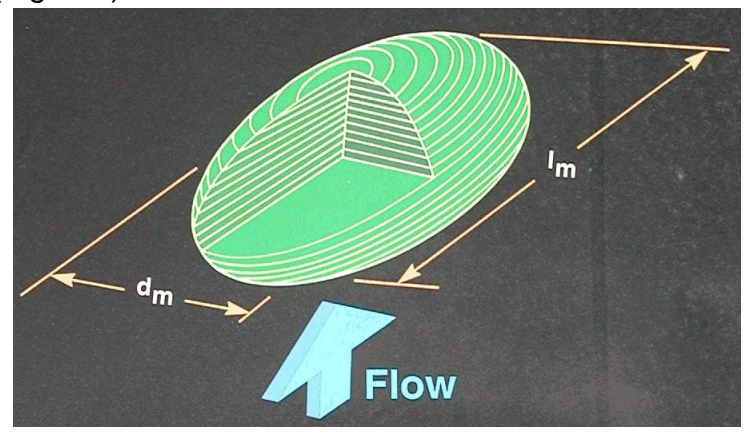


Figure9The intersection of the two beams forms an ellipsoid

Care must be taken to ensure that the seed is uniformly so that there is no asymmetry in the particle distribution. The particles must be small enough to give the flow of the studied fluid as accurate as possible. Another aspect related to the particles is that related to the diffusion of light. The LDV system avaiable at UTCB, is compose by Flow Lite with HeNe laser, 1 velocity component, and frequency shift; and a 2D FiberFlowAr-lon laser who have the possibility to measure 1, 2 or 3 velocity components, with frequency shift with the possibility to be added a wide selection of probes and accessories. The three YAG solid sources emit beams of 200mW, ad

different wavelengths 488nm, 532nm and 561nm. These are connected to a Burst Spectrum AnalyzerBSA Processor F/P 600 series.

The LDV system is used to measure the air velocityes distribution in the front of the inlets, these being imposed as the imput data in the numerical model.

## ► Hot wire anemometry

Hot wire anemometers use a very fine wire (on the order of several micrometers) electrically heated to some temperature above the ambient. Air flowing past the wire cools the wire. As the electrical resistance of most metals is dependent upon the temperature of the metal (tungsten is a popular choice for hot-wires), a relationship can be obtained between the resistance of the wire and the flow speed. The scheme of operating principle of the system of a hot wire anemometer is presented in Figure 10. Several ways of implementing this exist, and hot-wire devices can be further classified as CCA (constant current anemometer), CVA (constant voltage anemometer) and CTA (constant-temperature anemometer). The voltage output from these anemometers is thus the result of some sort of circuit within the device trying to maintain the specific variable (current, voltage or temperature) constant, following Ohm's law.

Hot-wire anemometers, while extremely delicate, have extremely high frequencyresponse and fine spatial resolution compared to other measurement methods and as such are almost universally employed for the detailed study of turbulent flows, or any flow in which rapid velocity fluctuations are of interest.

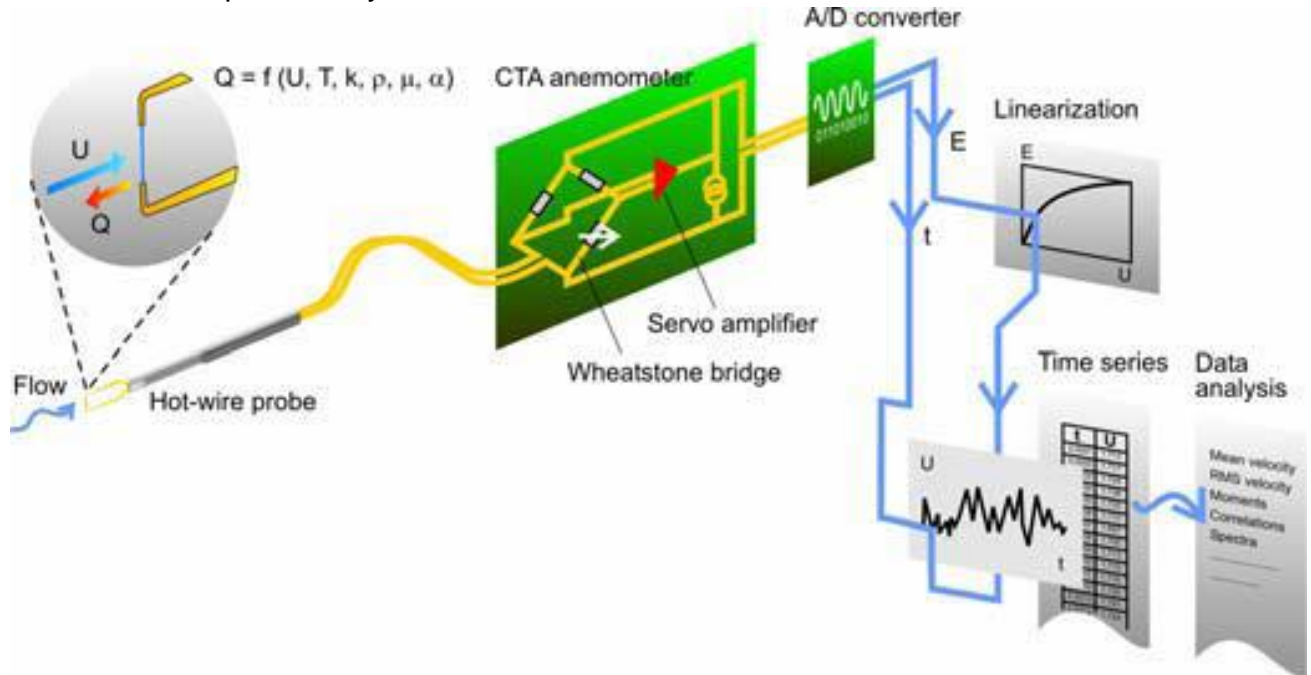


Figure 10. The scheme of operating principle of the hot wire anemometers

Considera wire that's immersed in a fluid flow. Assume that the wire, heated by an electrical current input, is in thermal equilibrium with its environment. The electrical power input is equal to the power lost to convective heat transfer

$$I^2 R_{\mathbf{w}} = h \cdot A_{\mathbf{w}} \left( T_{\mathbf{w}} - T_f \right)_{(2)}$$

where I is the input current,  $R_w$  is the resistance of the wire,  $T_w$  and  $T_f$  are the temperatures of the wire and fluid respectively,  $A_w$  is the projected wire surface area, and h is the heat transfer coefficient of the wire.

The wire resistance  $R_w$  is also a function of temperature according to,

$$R_{\mathbf{w}} = R_{\text{Ref}} \left[ 1 + \alpha \left( T_{\mathbf{w}} - T_{\text{Ref}} \right) \right]_{(3)}$$

Where a is the thermal coefficient of resistance and  $R_{Ref}$  is the resistance at the reference temperature  $T_{Ref}$ .

The heat transfer coefficient h is a function of fluid velocity  $v_f$  according to King's law,

$$h = a + b \cdot v_{f}^{c}$$
 (4)

where a, b, and c are coefficients obtained from calibration ( $c \sim 0.5$ ).

Combining the above three equations allows us to eliminate the heat transfer coefficient h,

$$a + b \cdot v_f^c = \frac{I^2 R_w}{A_w \left( T_w - T_f \right)}$$

$$= \frac{I^2 R_{\text{Ref}} \left[ 1 + \alpha \left( T_w - T_{\text{Ref}} \right) \right]}{A_w \left( T_w - T_f \right)}$$
(5)

Continuing, we can solve for the fluid velocity,

$$v_{f} = \left\{ \left[ \frac{I^{2} R_{\text{Ref}} \left[ 1 + \alpha \left( T_{w} - T_{\text{Ref}} \right) \right]}{A_{w} \left( T_{w} - T_{f} \right)} - a \right] / b \right\}^{\frac{1}{2} c}$$
(6)

## Other equipments

During the experimental sessions, besides those presented above, was used different temperature and humidity probes. For example, the interior surfaces and air temperature was monitorized with K type thermocouple network, for the mean radiant temperature a globe thermometer globe provide by testo was used. Regarding the humidity measurement, different higrometers was positionatein the vehicle cabin.

#### 1.2. Thermal comfortevaluation

For the termal comfort evaluation was used two equipamnets, each of them measuring different thermal comfort indexes. In order for the Predicted Mean Vote (PMV) and Predicted Percentage of Dissatified (PPD) a TESTO 480 equipment was used. While for the Equivalent temperature (teq) was used a advanced thermal manikin)

## ► Other thermal comfort assessment equipamnets

The at the data acquisition station TESTO 480 Figure 11 are connected different probes (air velocity probe, air temperature probe, mean radiant pemperature prove and relative humidity probe) are imposed the values of the clothing insulation and metabolic ratec and automatically are showe the PMV and PPD values.



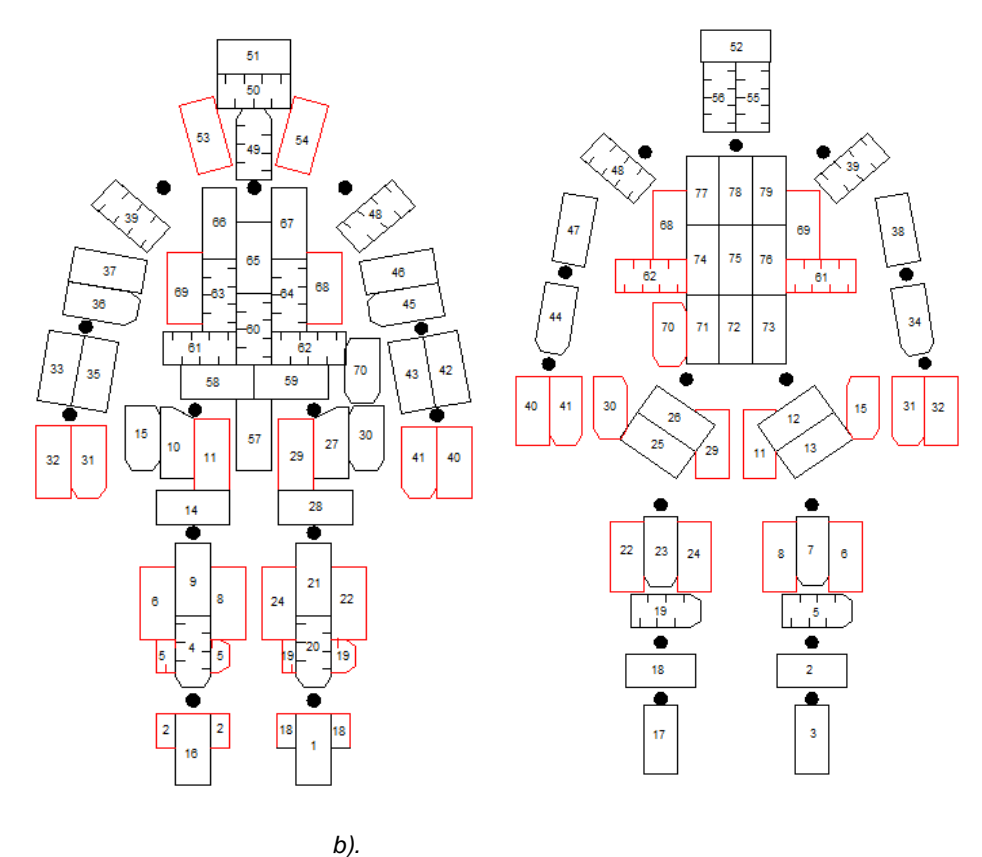
Figure 11. TESTO 480 thermal comfort evaluation tool

#### ► Thermal manikin

During the first year of doctorate studies I was directed involve in construction of an in house thermal manikin. This particular prototype is a female manikin, familiarly called Suzi. The thermal manikin has a human anatomical shape and the thermal control of the zones is realized with a neuro fuzzy system.

## Physical part of the manikin

Is devised in 79 zones (Figure 12) for each of these zones, can measure and controlled separately the temperature. Red zones are lateral zones, while the black points represent articulation points.



a). b). Figure 12. Arrangement of thermal manikin zones a). Front area; b). Backarea.

As a support is used a medical manikin made of polyvinyl, on whose surface was glued a thermal-insulation membrane from elastomer (see Figure 13). The function of this 5mm insulation membrane is to prevent the heat transfer from the manikin interior.



Figure 13. The medical manikin used

The thermal manikin is mobile, being able change position, in seated and standing postures. The size of the manikin is a standard human size with a total surface of 1.8m<sup>2</sup>. The heating solution chosen for this prototype consist in using six types of elementary patches (Figure 14) that are combined to cover each individually controlled

zone.

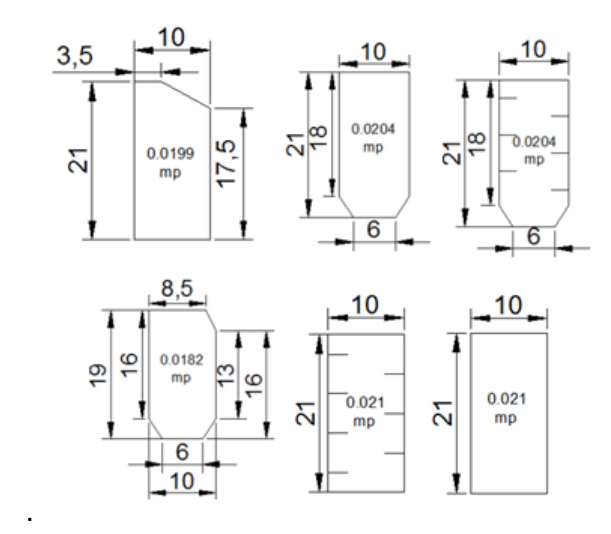


Figure 14. Shapes of heating elements used

The heating elements, consist in an electrical conductive metal (made of nickel chrome) arranged curvilinear Figure 15.a, placed between two layers of flexible material, having good electrical isolator proprieties and in the same time is a good thermal conductor Figure 15b. The heaters are flexible elements and allow bending on the humanoid manikin shape.



Figure 15 a. Internal heater element structure; b. Heather

Several solutions of films and heating materials were tested but the heating silicone patches were found to provide the best uniformity in terms of temperature distribution. The heating film patches were placed on the insulation layer of the manikin base, using with double side adhesive tape.



Figure 16. Temperature sensors stick on heating elements

To measure the surface temperature, five temperature sensors was stick on each hetingpach. Each temperature sensor was gresed with thermo-conducting paste with

silver particles to ensure the heat transfer from the pachFigure 16. Because the sensor size is very small, their place on the heating element was fixed with a infrared camera Figure 17. In this way was removed the danger of have inaccurate mean temperature. Also for a better contact with the heating element, a thin layer of thermal grease was applied on the surface on each temperature sensor.

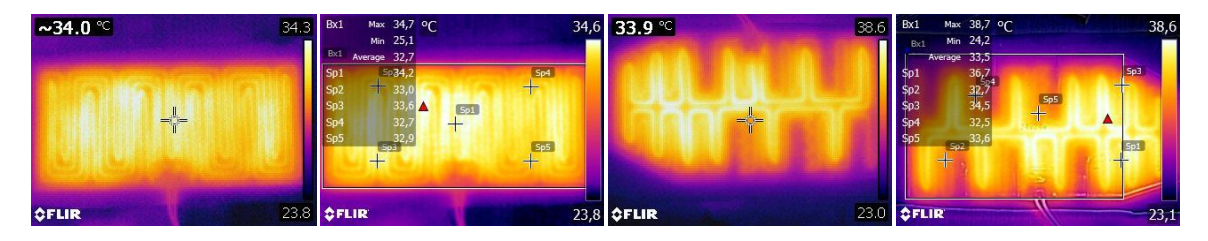


Figure 17. Infrared images of the heating elements

As a non-uniform temperature of the manikin surface has to be avoided we decide to cover the entire manikin surface with adhesive aluminum foil (see Figure 18b) to ensure enhanced conduction heat transfer. Finally, in order to facilitate further investigations with a thermal (IR) camera the entire manikin surface was covered with a transparent adhesive film. In order to validate the heating part of the manikin prototype we performed several tests, concerning the distribution of the surface temperature of each manikin, the sensors employed for the control part, the electrical characteristics of the used components.InFigure 18a, are compared the surface temperature distributions of a flexible polyamide heating film, of a silicone patch and of the human skin of the hand

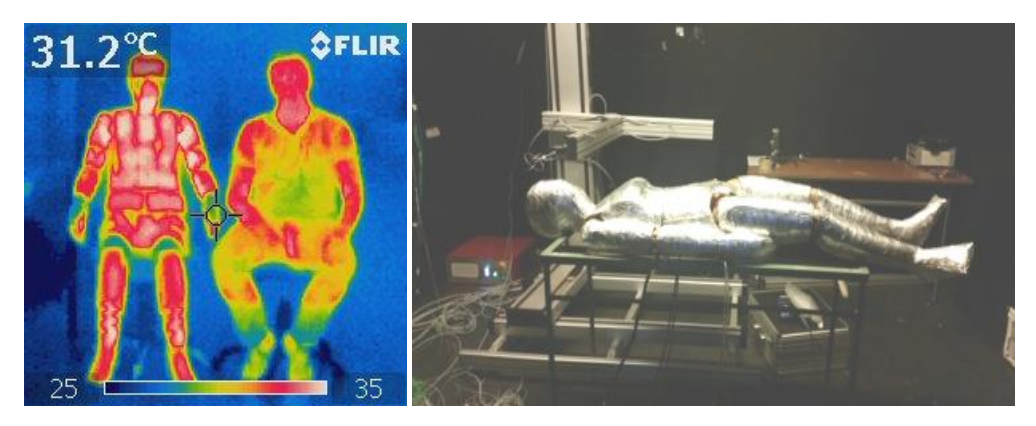


Figure 18. a). A comparison between the surface temperature distribution of the manikin and the human clothed body; b). the thermal manikin with aluminum foil

After covering a body zone the electrical connections and circuits were created. Every electrical connection was tested for leakage for safety reasons. The electrical wire was embedded inside the manikin. In order to ensure that the thermal load of the film mounted over the wires is not influencing the cable stability we selected special electrical wire that works at temperatures above 7°C.

During a preliminary test, without any control of the circuits, the temperature of each zone stabilized at 45°C when the room temperature was stable at 24 °C, a rather encouraging result offering a wide range to control the temperature of each zone and the possibility to simulate different cases of body heat release

Architecture of the control system of the thermal manikin

The thermostatic manikin system consists of 79 patches each with a heating element (24 Ohms constant resistance) and 5 analog temperature sensors (TSic 501) mounted on each patch surface used by the control system to maintain a constant preset temperature of the manikin surface. The 395 acquisition channels are collected by the multiplexer interface (Figure 19) to help miniaturizing of the electronic system, by reducing the space occupied by wires, thus being able to fit inside the manikin.

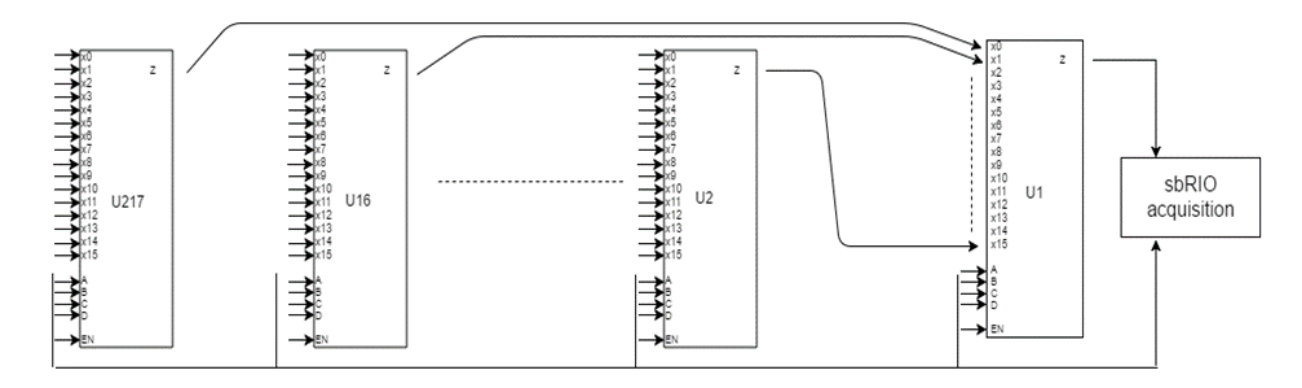


Figure 19. Multiplexer simplified circuit diagram

For the development of the system there were used two boards from National Instruments (myRIO 1900 and sbRIO 9363). Both have a unit of sequent calculus (x86) and unit of matrix calculus. To connect the temperature sensors to the development board there was used a multiplexer interface based on HEF4067B. The control of the MOS transistors used for the execution system was achieved through an interface made of SN7407 circuits. Basic architecture of the manikin system is given in next figure.

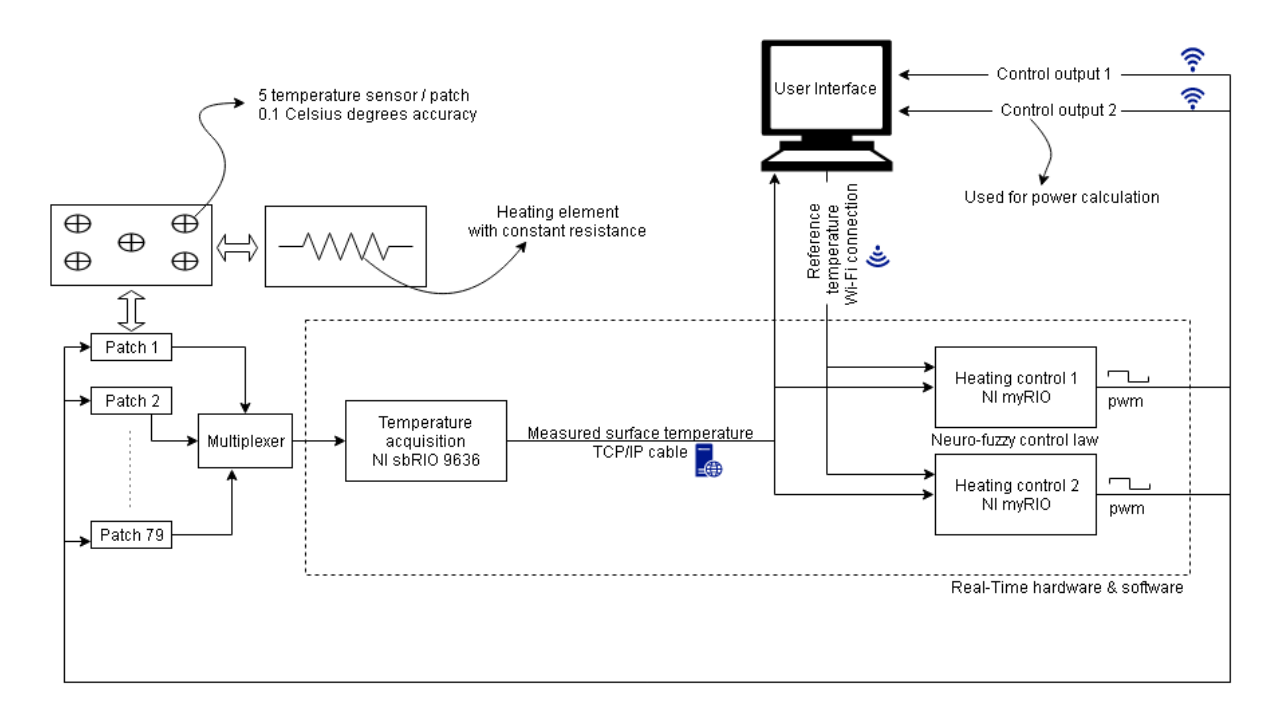


Figure 20. Basic architecture of manikin system

The FPGA software on the sbRIO 9636 handles the acquisition of data from the multiplexer interface which, instead of requesting one input at a time, collects all the inputs and separates them by shifting the register in the temperature data memory. The software from myRIO 1900's FPGA creates the PWM pulse used to control the patch surface. Both NI boards have implemented real-time software, the acquisition device also processes the data to obtain reliable mean temperature of every patch using a fault detection and isolation algorithm, while de heating control devices, using the data processed by the acquisition board, generate robust and adequate signal using the neuro-fuzzy controller. The real-time hardware and software can run independently from the computer user interface, with the limitation of maintaining the last (or default) requested set point of temperature.

The computer software allows the user to load set points for several testing situations, change the set point on each patch independently and monitor the behavior of the temperature data and control system. The user can also view the average equivalent temperature displayed graphically on a simplified model of manikin and average power consumption.

The necessity of processing a high amount of information (395 acquisition channels, signal filtering, etc.) and generating proper signals for 79 command channels, as well as the strict timing, provided by the NI boards Real-Time processor and required for the control of electronic circuits (multiplexer and MOS driver interface), lead clearly to the conclusion that this technology is the best solution for the manikin system. The control algorithm for the command channels was converted into software for the sequent calculus unit of the NI boards.

Block-schema for the control of one channel is shown in Figure 21. PWM (pulse width modulation) is a well known technique to produce analog signal using digital devices that output a square signal by switching on and off the output port. By modifying the period that the signal is on and off, a voltage between 0 and 24V (the maximum voltage recommended for the patches) can be simulated. Since myRIO 1900 boards can output only 3.3V in DIO (digital I/O) ports, there has been added an interface to convert 3.3V TTL signal to 5V CMOS signal needed by the transistors to open and close the 24V supply circuit according to the PWM control generated by the neuro-fuzzy controller. Artificial intelligence based approach in the treatment of control problems concerns in principle an input-output behavioural philosophy of solution.

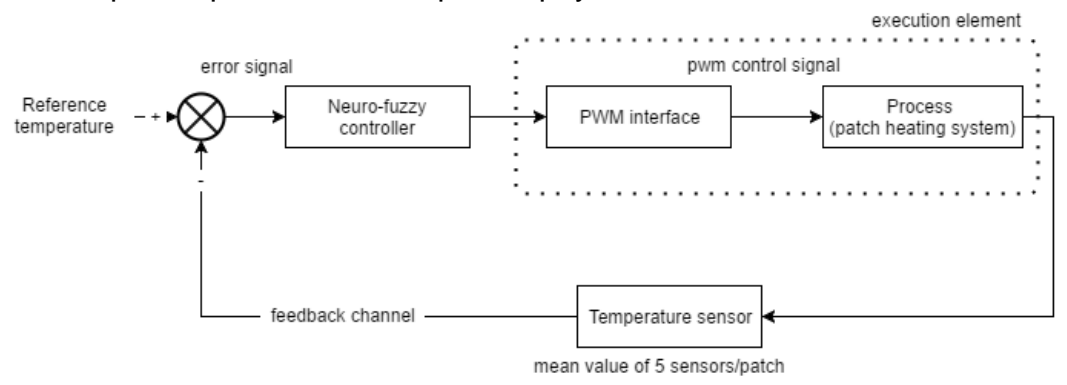


Figure 21. Control system diagram for one control channel

## Manikin's thermal comfort indicators

The equivalent temperature that represents an indication of thermal comfort is obtained by evaluating the power consumption of a region of the manikin. Due to the pwm control signal which commutes on and off between maximum and minimum voltage, the power consumed by the thermostatic system was calculated by creating a calibration slope between pwm duty-cycle and the power calculated as a point by point mean of a single pulse period. The voltage drop on the patch was calculated differentially by measuring with the Hantek DSO5102P oscilloscope thevoltage drop on the whole circuit from which it was subtracted the voltage drop on the transistors. The current consumed by the patch was measured with TH5A current transducer.

$$\theta_{ech} = \theta_{reg} - \frac{P}{S*h_{calc}}(7)$$

Where  $\theta_{ech}$  = equivalent temperature;  $\theta_{reg}$ = mean temperature of surface region calculated using a sliding average over a preset period of time; S = surface area of manikin's region; P = mean power consumption calculated using a sliding average over a preset period of time;  $h_{cal}$ = convection coefficient calculated with equation at constant environment temperature ( $\theta_{ech}$ ) of 24 °C and manikin's surface temperature controlled at 34 °C.

Experiments revealed that by modifying the environment temperature from 20 to 40°C the changes in power consumption were indistinguishable Figure 22

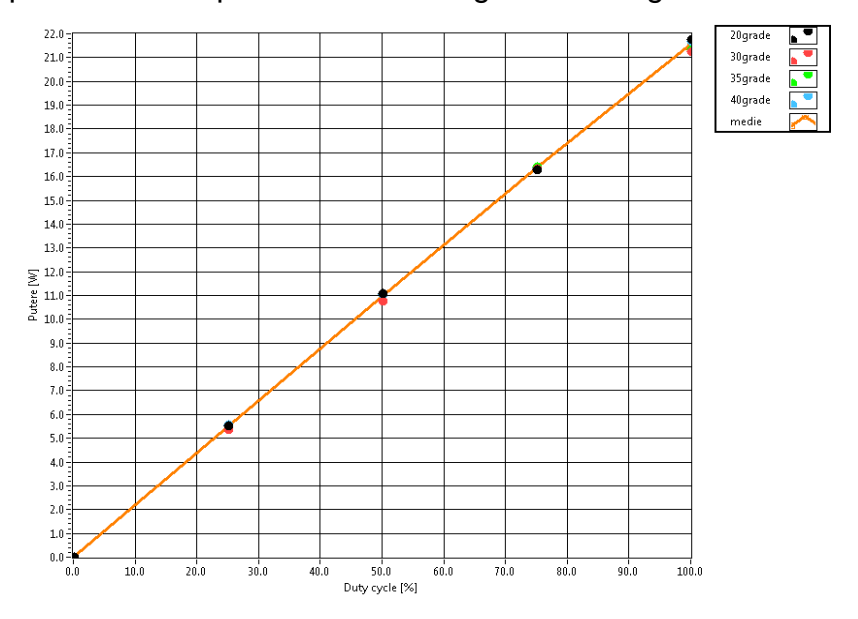


Figure 22. Power variation as function of PWM duty-cycle

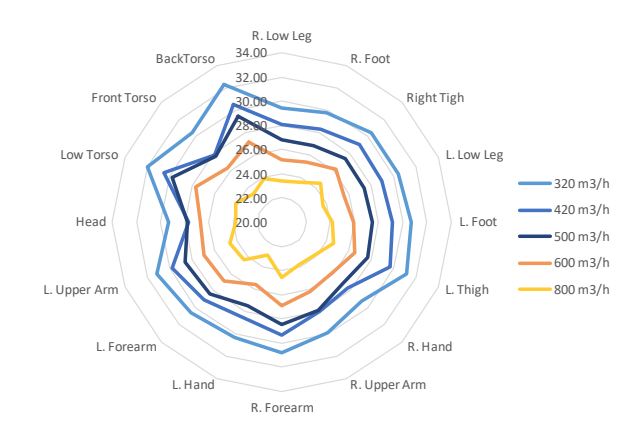


Figure 23. Example of  $\theta_{ech}$  distributions obtained from the thermal manikin data for several air flows

Compared to classical measurement systems which give the possibility of estimating the global PMV, the thermal manikin gives the advantage of assessing locally a predicted local sensation, either through the equivalent temperature either through a derived local PMV. The thermal manikin represents a worthy tool for the thermal comfort analysis in laboratory configurations and in real field case studies being a method of investigating local discomfort trough the local distributions of the equivalent temperature of the segments of the manikin. This kind of representation allows for instance, the inspection of the uniformity of an environment. In Figure 23, we show an example of equivalent temperature distributions for several air flows defined by Nilsson [10-12] or in the standard EN ISO 14505/2 [13] for a studied air grille for operating rooms.

## III. Numerical model construction:

The numerical model was developed under the direction of Associate Professor Florin Bode and in collaboration with Technical University of Cluj-Napoca (UTCN). Construction of the numerical model was divided in a few steps.

▶ The first step - Generation of the Megane geometry and the grid for the computational domain. This first model did not include the human geometry. The car geometry was designed in Catia software and then imported in Ansys DesignModelerin order to be prepared for the numerical simulation. Mesh generation was realized the same in Ansys. A mesh independence study was carried out (Figure 24). A poor quality grid will cause inaccurate solutions and/or slow convergence. More cells can give higher accuracy. The downside is increased memory and CPU time. In this case the choosen numerical mesh grid was composed of 6.1 million elements. The elements are tetrahedral due to the complexity of the geometry. The boundary layer consists of 5 layers. The grid independence test was carried out on five different grids: 1.2, 2, 4.8, 6.1 and 8 million elements. The numerical results obtained with the 6.1 and 8 million elements showed small differences so we choose the 6.1 million elements grid from computational reasons.

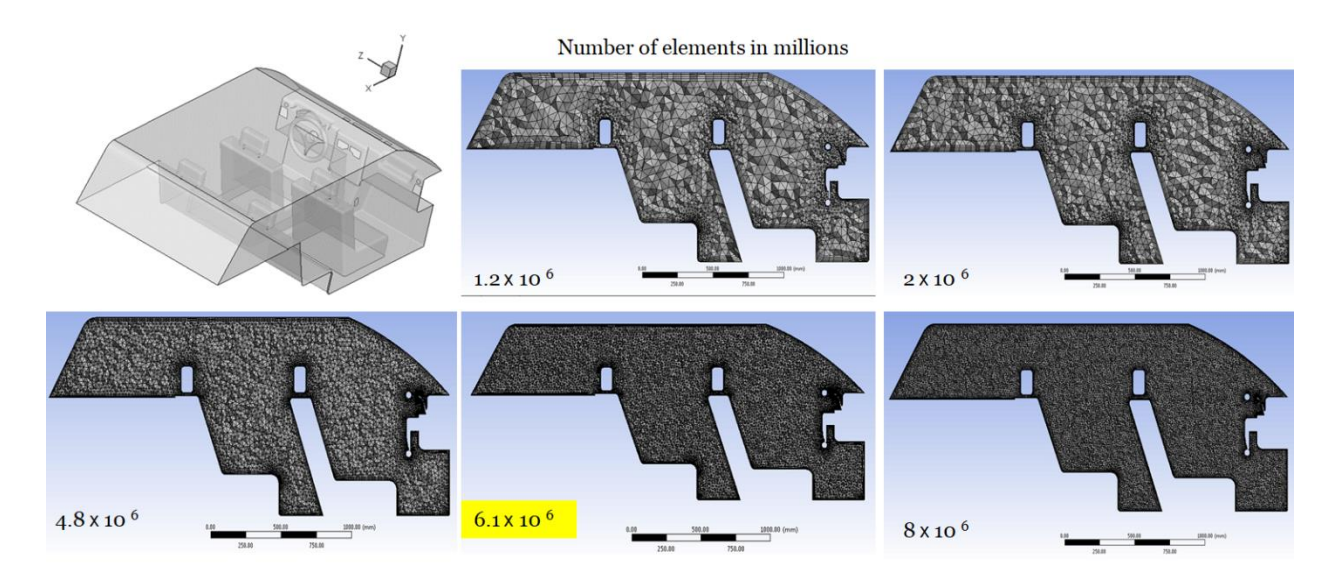


Figure 24. Numerical grids used for the mesh independence study of the numerical model without thermal manikin

▶ The second step was validation of the numerical model. Validation is the process of determining the degree to which a model is an accurate representation of the real world from the perspective of the intended uses of the model. Validation deals with the assessment of the comparison between sufficiently accurate computational results and the experimental data. The necessary data for this the second step was obtained from

an experimental measurement session. Most of the experimental studies having the purpose to validate numerical models of the passenger compartment that are available in the literature, have been conducted in spaces in which, was attempted to maintain constant the values of thermal parameters [referinta]. In this case the boundary conditions imposed to the model, can be imposed also to the experimental facility. In our case, the boundary conditions imposed to the model were data obtained through measurements on the defining surfaces and related to the air flows.

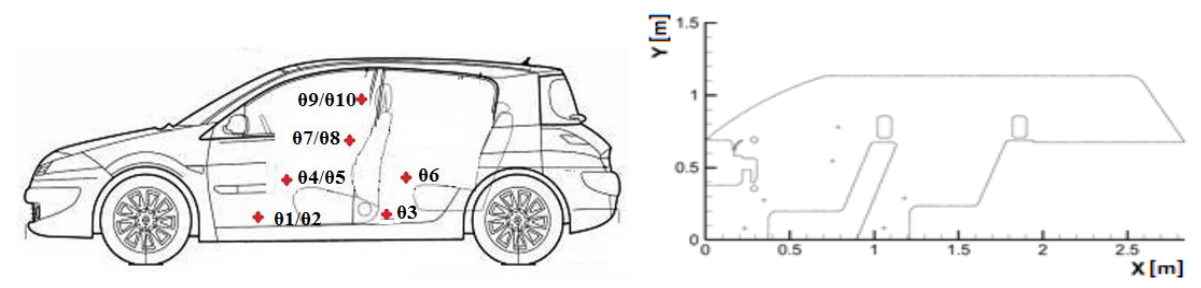


Figure 25. a). K – type thermocouples at different passengers position b). monitored points in CFD model;

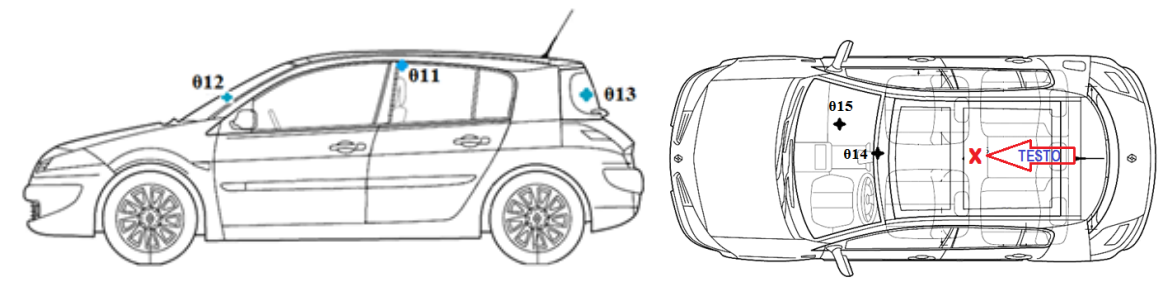


Figure 26. Measuring points with K- type thermocouples, on different cabin surfaces

During the experimental session of measurement, the automobile (Figure 25 and Figure 26) was placed in the aforementioned hall, protected from outside weather conditions. Measuring sessions were conducted in days with temperatures relatively similar, so both outside in the hall and inside cabin temperature has constant values between 21-24.5 °C. For the choice of our boundary conditions we considered only cases where the temperature evolutions inside the cabin car were constant in time (seeFigure 27). It can be seen that the variation during the considered measurement session is insignificant for all the measurement points. A network of 15 K-type thermocouples was used to monitor variation of temperature on different surfaces of vehicle and in different places where normally human body parts are (head, chest, knee, foot). The K-thermocouples were positioned as inTable 1, Figure 25. andFigure 26.

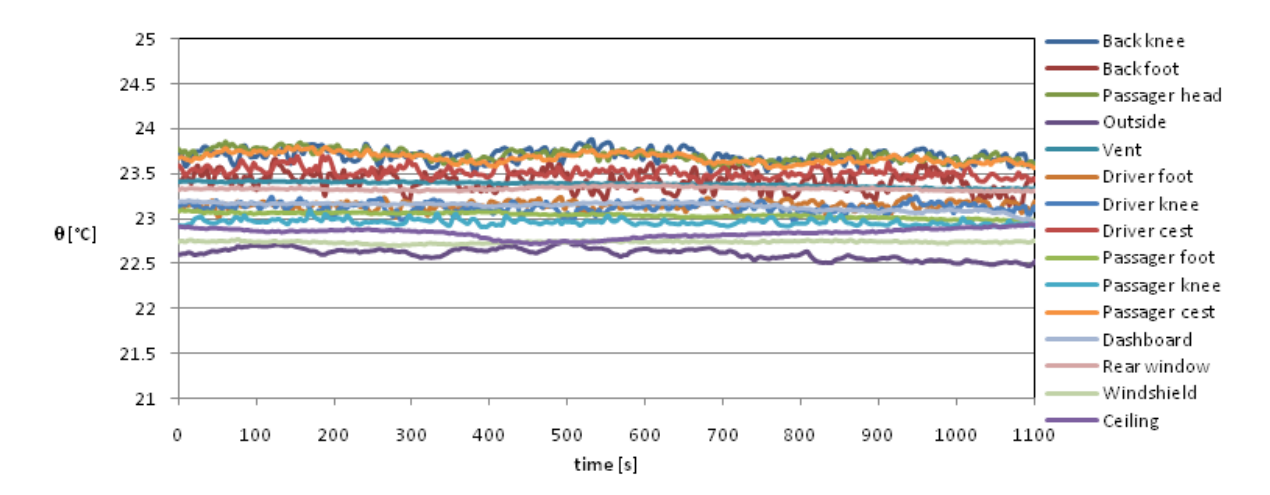


Figure 27. Example of temperature variation inside the cabin for the considered boundary conditions

Table 1. Sensors positions legend

rabio ii Collecto prometto legena									
No	Place of installation								
θ1	Diver foot								
θ2	Front Passenger foot								
θ3	Back foot								
θ4	Driver knee								
θ5	Front Passenger knee								
θ6	Back knee								
θ7	Driver chest								
θ8	Front Passenger chest								
θ9	Driver face								
θ10	Front Passenger face								
θ11	Ceiling								
θ12	Windshield								
θ13	Rear window								
θ14	Vent								
θ15	Dashboard								
	<u> </u>								

Various other sensors (air velocity, relative humidity and mean radiant temperature) were installed in vehicle cabin, to monitor other parameters whichinfluencethe thermal comfort. To obtain the air flow rates a TSI Flow meter was placed in front of each discharge grille with an adapted convergent nozzle. Also, in places where human body parts should be, the air velocitywasmeasured with an omnidirectional probe and the local temperature values with a thermistor that is embedded in the same instrument. The two sensors are part of a TESTO 480 instrument. During the experimental approach a total number of 12 measurement sessions were carried out, each session lasting 50 minutes. During measurements, we usedonly body discharge grills, the inlet velocity speed regulator of the vehicle HVAC system was posinitioned nthe second position of the total of four. Using TSI flowmeter, flowrate from every discharge grill was determinate.

We used the data from from the experimental measurement sessions to impose the boundary conditions for the numerical model. We imposed a mass flow rate of 0.041856 kg/s on the central grills and a mass flow rate of 0.0394766 kg/s on the sides grills. Air temperature at the inlet grills was imposed as 23 °C. The inlet turbulence intensity was imposed as 4.11% being calculated using the empirical relation proposed by Jaramillo [14]:  $I = 0.16 \, \mathrm{Re}^{-1/8}$ .

The Reynolds number at the exit of the central orifices based on streamwise mean velocity and equivalent diameter ( $D_{e1}$ = 0.092963m) was Re= 17763, and for the sides grills Re= 13924 ( $D_{e2}$ = 0.072871m). For the pressure-velocity coupling we utilized the COULPED algorithm. A second order upwind scheme was used to calculate the convective terms in the equations, integrated with the finite volume method. For the near-wall modeling, the standard wall function was used. The turbulence model used for the numerical simulation was RNG k- $\epsilon$ , because the overall performance of this model is one of the best for the indoor environment modelling [15, 16]

To validate our model, we compared air temperature and velocities in the considerate points. As is shown is inFigure 28, the differencebetween experimental measurements and numerical results for the air velocity and temperature are very small. These similarities lead us to the conclusion that our numerical model is validated.

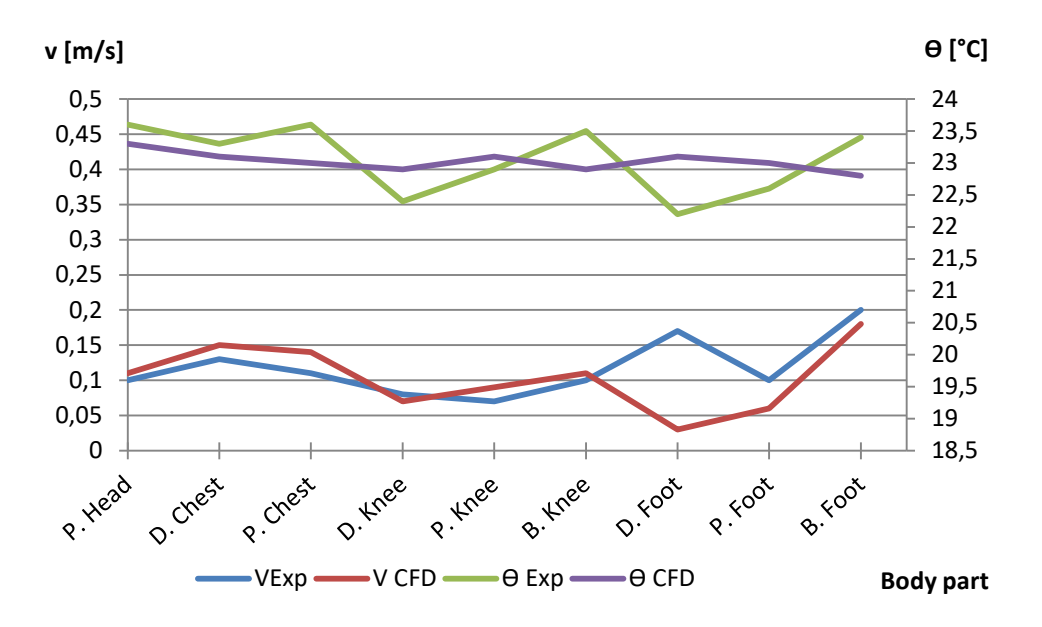


Figure 28. Comparison between experimental and numerical resupts for the air velocityand temperature in the automobile

Also, forthe validation purpose, PMV and PPD indices were calculated forboth cases, imposing metabolic rate value of 1 Met, constant clothing insulation resistance value of 0.7 clo and relative humidity of 60%.

Point/parameter of	PMV		PPD	
measurement	Exp	CFD	Exp	CFD
Passenger Head	-0.38	-0.48	8.11	9.80
<b>Driver Chest</b>	-0.54	-0.65	11.24	13.91
Passenger Chest	-0.42	-0.63	8.73	13.26
Driver Knee	-0.58	-0.48	12.03	9.91
Passenger Knee	-0.47	-0.45	9.71	9.29
Back Knee	-0.40	-0.55	8.37	11.43
Driver Foot	-0.88	-0.45	21.51	9.29
Passenger Foot	-0.57	-0.47	11.79	9.59
Back Foot	-0.70	-0.79	15.29	18.40

▶ The third step - introduction of a virtual thermal manikin in to the cabin model

From the beginning several issues were encountered, one of them being the small space from the cabin. Another issuewas the position of the manikin. The generated manikin it would be like in the driving position with a hand on the stearingweel and as much as possible introduced in to the seat to avoidnarrow spaces formation which will lead to mesh of poor quality in those areas.. After several trials a human virtual body was modified from a freeware version found on internet. To be in a proper position and stikto the seat, the manikin body was modified in Catia and then imported to Design Modeler.

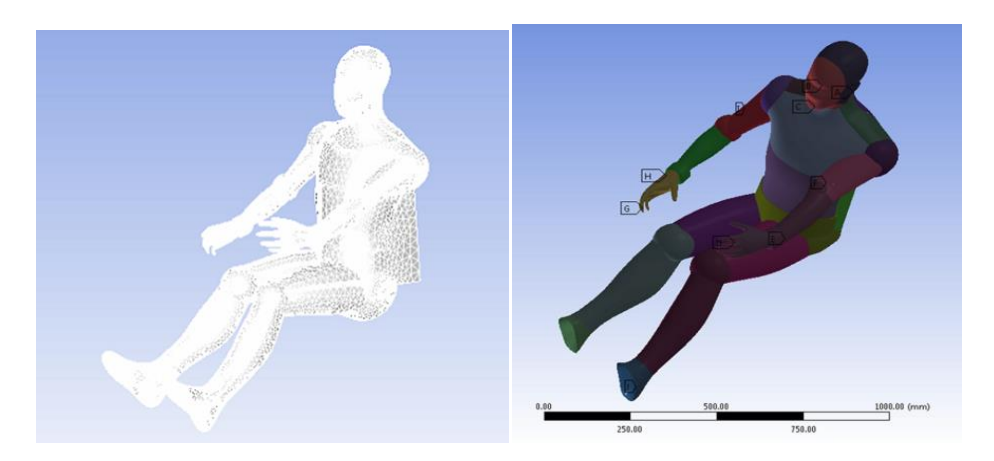


Figure 29. Virtual manikin zones

Before the fitting in the cabin geometry, the manikin was first meshed and tested in a virtual box, to simulate the evolution of the thermal plume Figure 30. The imposed temperature on the manikin surface was 34°C and the ambiental temperature 24°C at the air velocity 0. The surface of the virtual manikin was divided in regions in the same way as the real thermal manikin (see Figure 29) and fitted in the megane geometry.

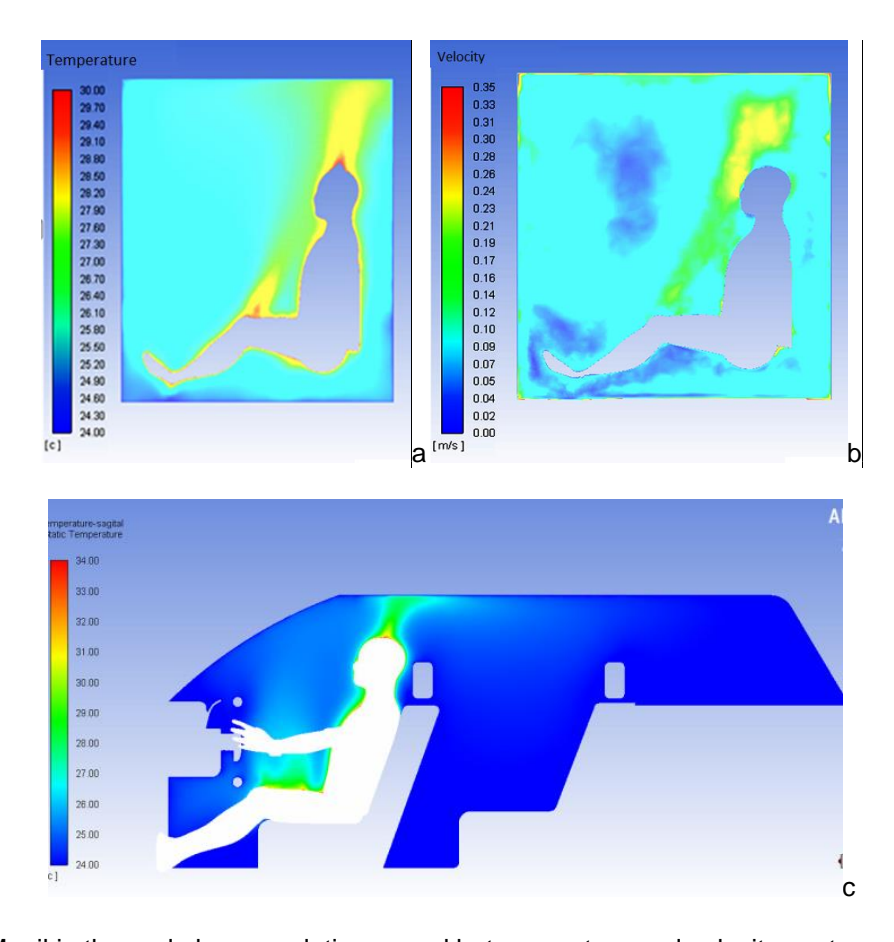


Figure 30. Manikin thermal plume evolution a. and b. temperature and velocity contours for the virtual manikin placed in the testing box, c. temperature contours for the case with the virtual manikin introduced in the automobile

Several meshes with tetrahedral elements where tested to check the independence of the solution (Figure 31). We choosethe mesh with 6.54 million elements.

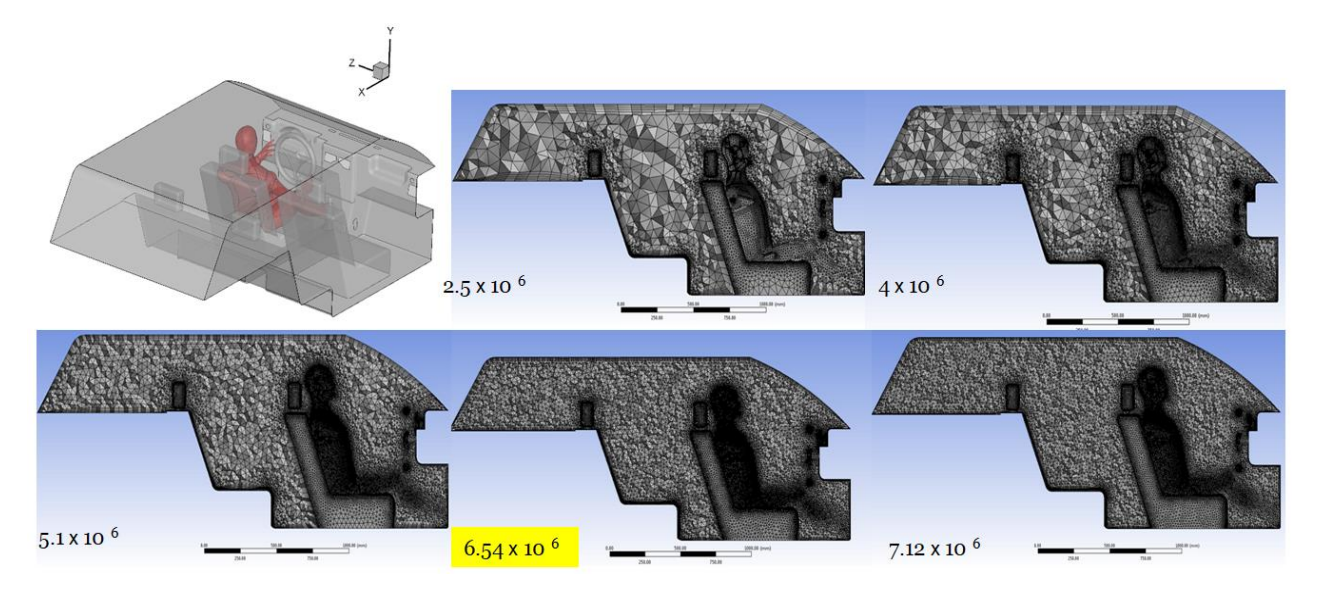


Figure 31. Numerical grids used for the mesh independence study of the numerical model with virtual thermal manikin introduced (driver position)

▶ The fourth part is presenting validation of the numerical model with virtual thermal manikin introduced (driver position). The purpose was to validate through comparation thermal states of the experimental (Suzy) and the numerical manikins. Therefore, an experimental session with the thermal manikin Suzy in the cabin was carried outin order to have imputsdatas and also validation datas for the numerical model. Temperature, velocities and equivalent temperatures were compared to check the validity of our model.

For the first numerical model validation, the flow rate velocity profile from the inlet grill was considered to be uniform. A shortcome of this work ipothesis is that the same velocity on the entire inlet surface is not a realistic case. In the literature were published articles that are studying the effects of duct shape over the airflow distribution in the vehicles. The conclusions were that the airflow velocity distribution on the air vent openings is not uniform. The airflow directivity within a vehicle cabin is mainly influenced by the air duct orientation, number of air vents, shape and positions. Considering a uniform air velocity as boundary condition is changing the airflow distribution from the vehicle cabin and in turn the thermal sensation of passengers may differ. The competition for space in new vehicles is intense, so the HVAC ducts are often squeezed between different components and the ducts geometry is very complex. In Figure 32is presented the ventilation duct system for our vehicle.



Figure 32. Renault Meganeducts geometry

To impose the real air velocity distributions at the inlet grills we need to determinate it.

The first idea was to drow these ducts and to simulate the flow of air through them. Using a 3D drowingsoftweare, left and right ducts was drown, these are presentd in Figure 33. But this procedure for determining the inlet velocity distribution stoped from the early stages because these ducts have many details and in the meshing process appeared some problems. The duct shape is very complex and the design optimization is not an easy task to be performed.

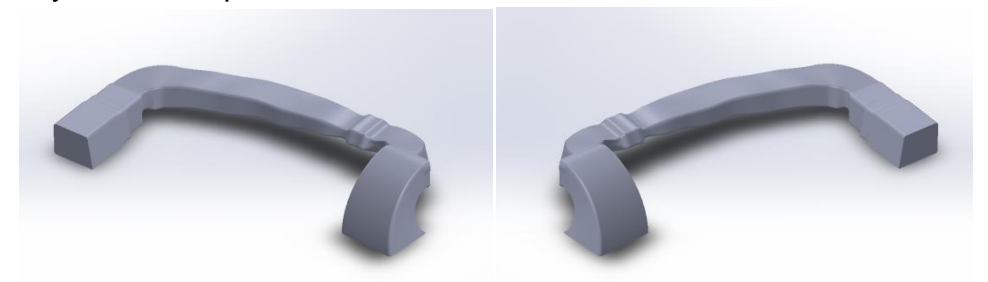


Figure 33. the megane geometry ducts drown in SolidWorks

The second idea was to determinate the velicitymap, trough Laser Doppler Velocimetry measurement, using the measurement system described above. To facilitate our work ahashboard including all ventilationsystem from a Renault Megane carwas purchased. The dashboard was mounted on a specially designed support to ensure mobility (see Figure 35 a).

Before measuring, the LDV system was calibrated. This calibration consists in aligning the probes, such that the beam intersection for the three components to be in the same point. Using a pin hole (Figure 34), the probe position was fine changed in order to align the intersection points.

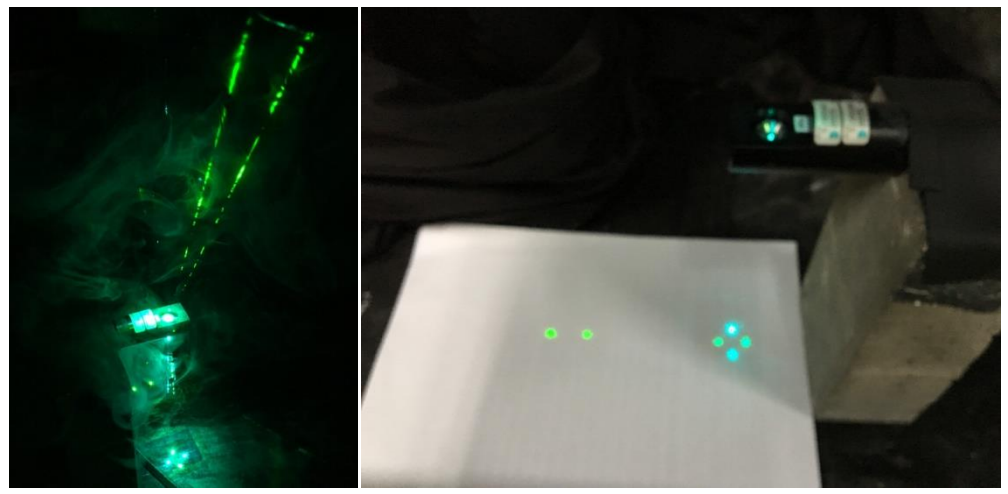


Figure 34. laser meabs passing trough pin hole



a). b). Figure 35. LDV measurements in the front of middle grills

As a measurement protocol, several velocity distribution profiles was meashuredatdifferet distances from the outlets, in the orisontal and vertical plane as is shown in Figure 36. Anstep of 5 mm was imposed between the measurement points. Starting from defined point 0; 0; 0 thevelocity distribution planes on X(u), Y(v) and Z(w) axes was meashred. To move the two measuring probes a displacement a traverse was used. The nearest measuremet grid was at x = 14 mm from the blower face. The oval shape of the board did not allow getting closer. The nearest velocity map is used as boundary condition for the numerical model, the others being used to validate our numerical model.

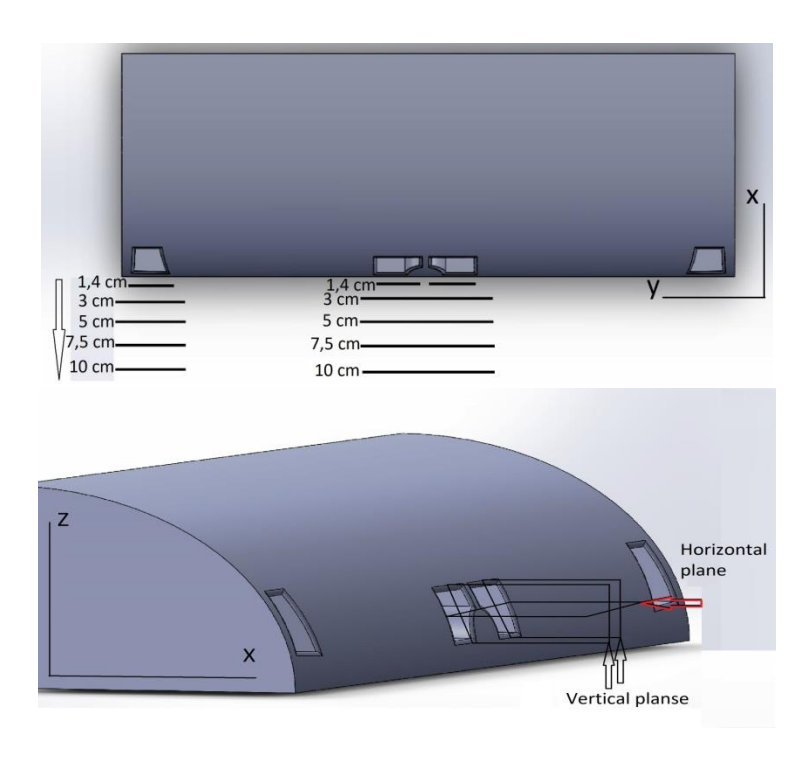
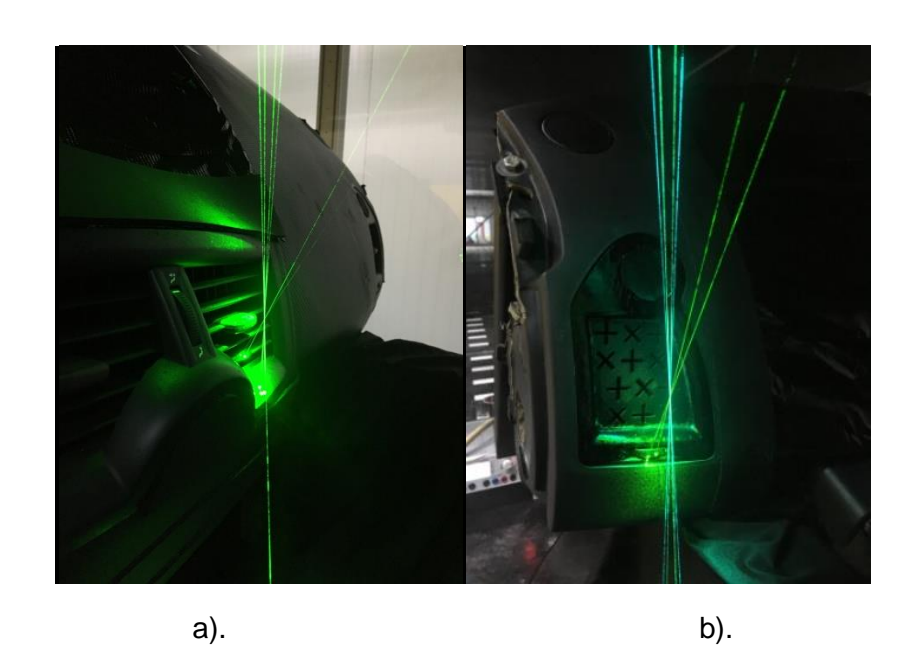


Figure 36. Velocity measurements planes

These velocity profile measurements are made for several grills models. The first model are the classical grills (Figure 37 a), the second model are with cross-shaped holes (Figure 37 b), the third model is consisted in a sphere with a single hole with daisy geometry(Figure 37 c), the forth model have the directional blades lobed (Figure 37d).







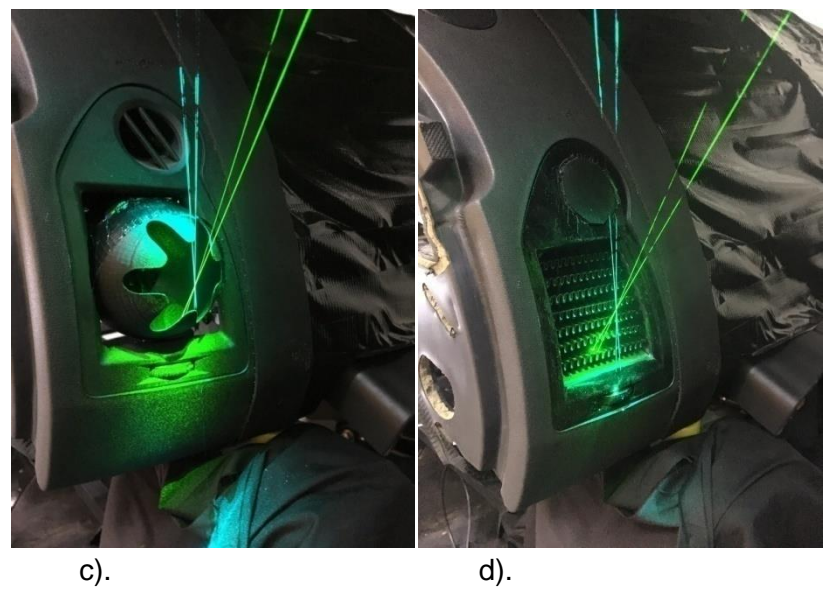


Figure 37 inlet types a). classical; b) cross-shape holes; c) sphere; d) lobed blades

The new inlet geometries were designed and manufactured in our laboratory. These were drowning using SolidWorks 3D software then imported in 3D Simplify software to be prepared to print. These are made of (PLA) Poly-Lactic Acid, it is a thermoplastic polymer which was processed by German RepRap X400 3D printer.



Figure 38.New grills design



Figure 39.images during the printing of the new grils



Figure 40. the new printed blowers before painting

After printing the new outlets geometries, was placed in the place of the classical straight blades before painting with black color.



Figure 41. blades lobeds grill before painting

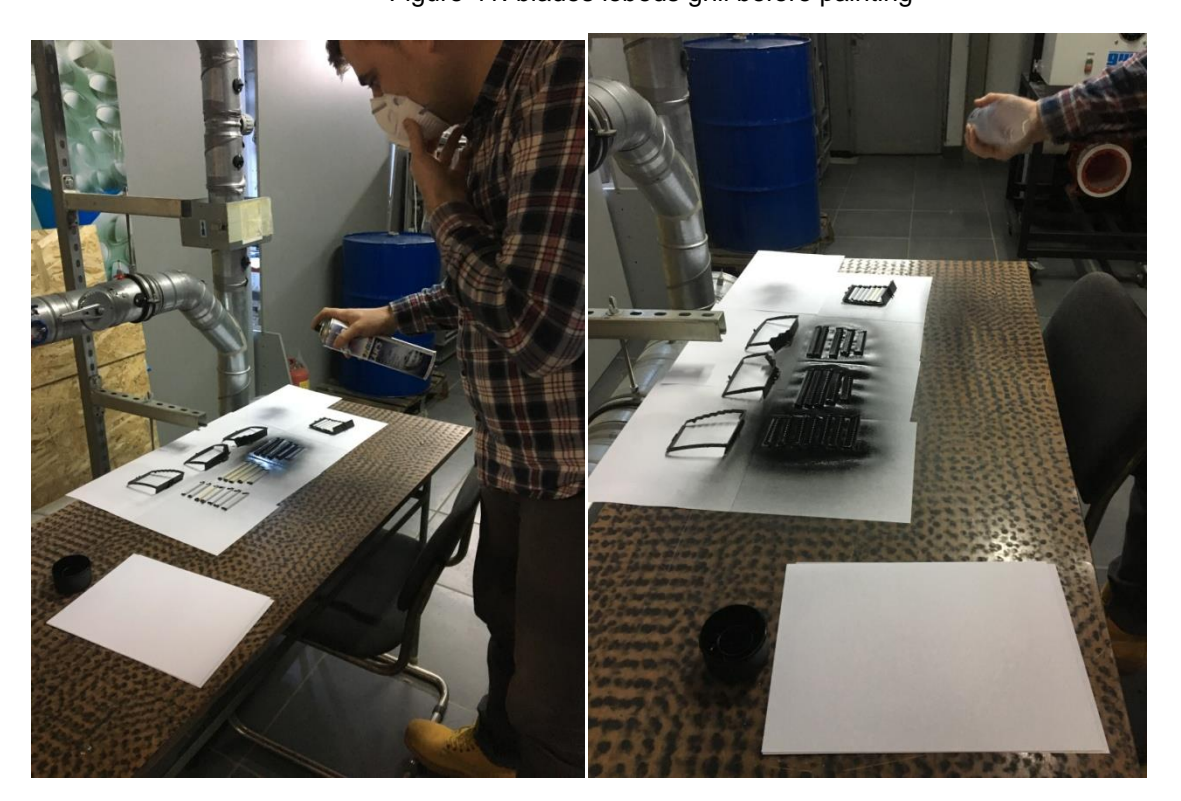


Figure 42. pictures from the printing process.

The LDV 3D – measurement equipament used, is manufactured by Dantec and is composed from a 2D FiberFlow laser with wavelengths of 488nm and 514nm; an 2D FlowLitewith wavelengths of532nm. These are connected to a Burst Spectrum Analyzer BSA Processor F/P 600 series (Figure 43). With a RS 323 the processor is connected to a computer, used to setup the measurements planes. The two measurement probes was fitted on a traverse system.

After the measurement each plane was exported as .xls file. To treat them, Tecplot software was used.



Figure 43. 3D-LDA measuremet system used

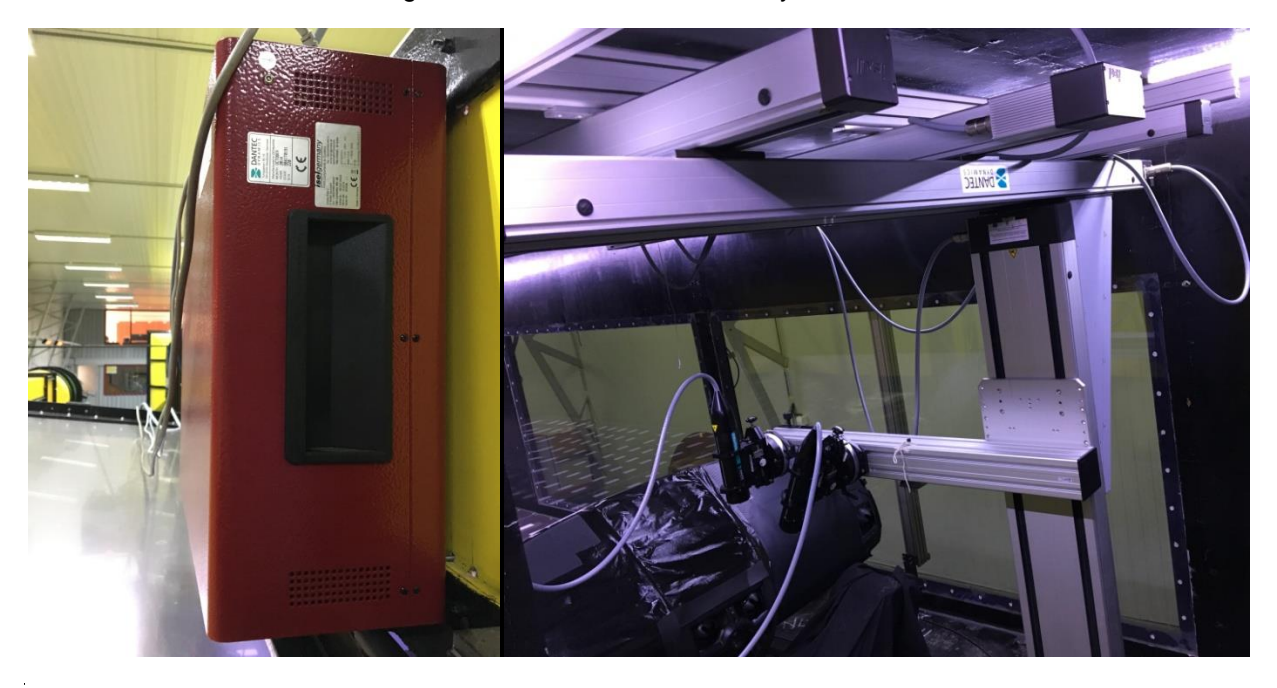


Figure 44. traverse system used

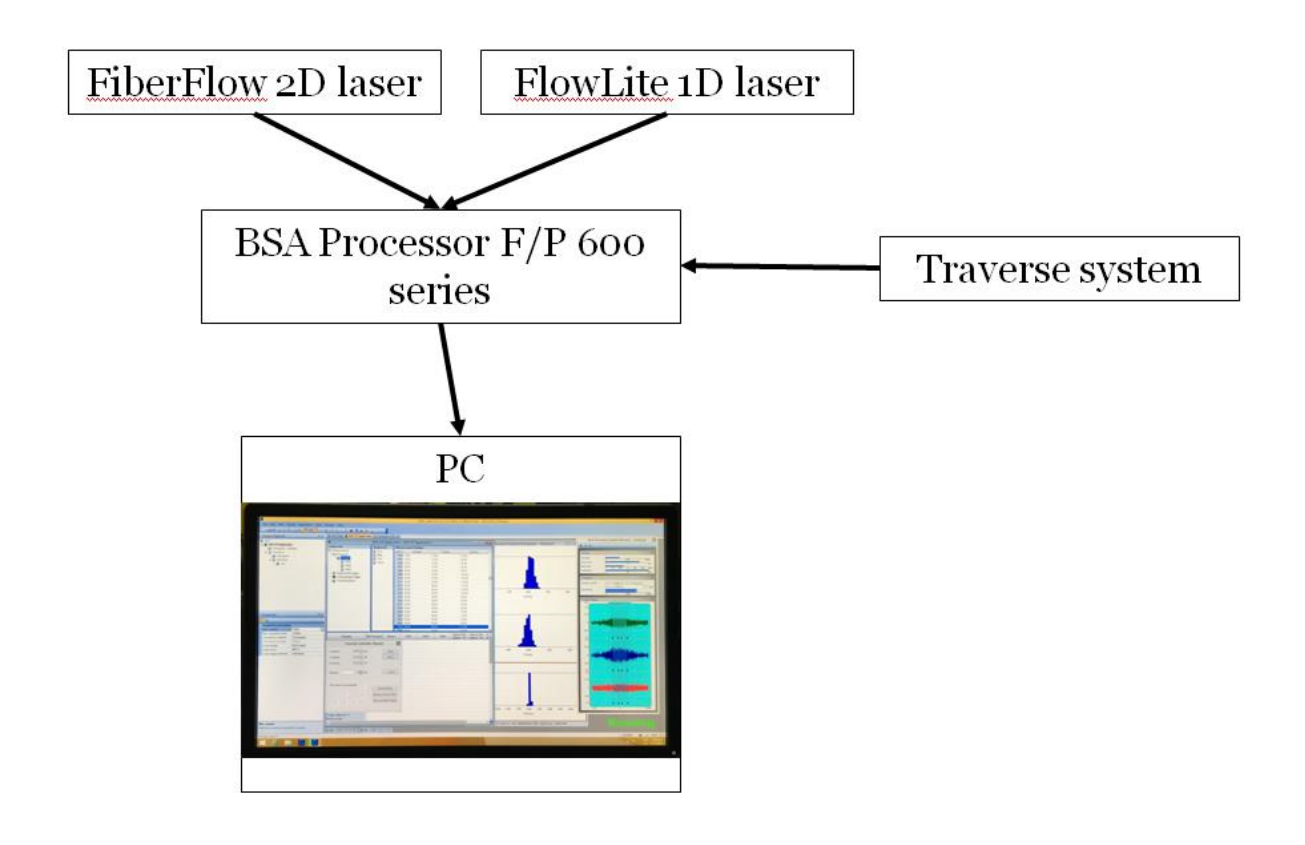
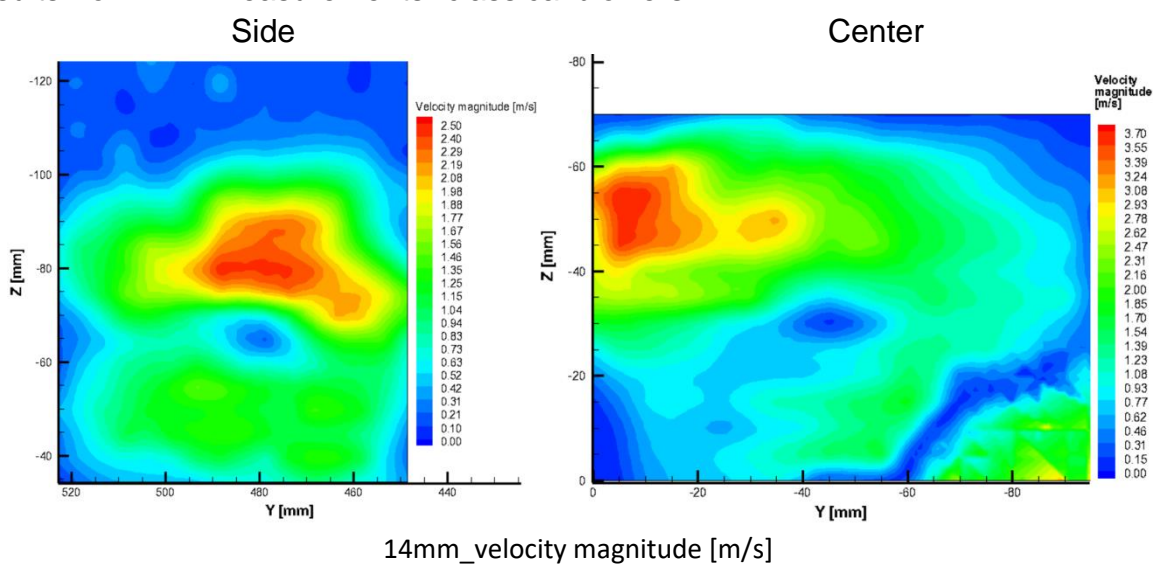
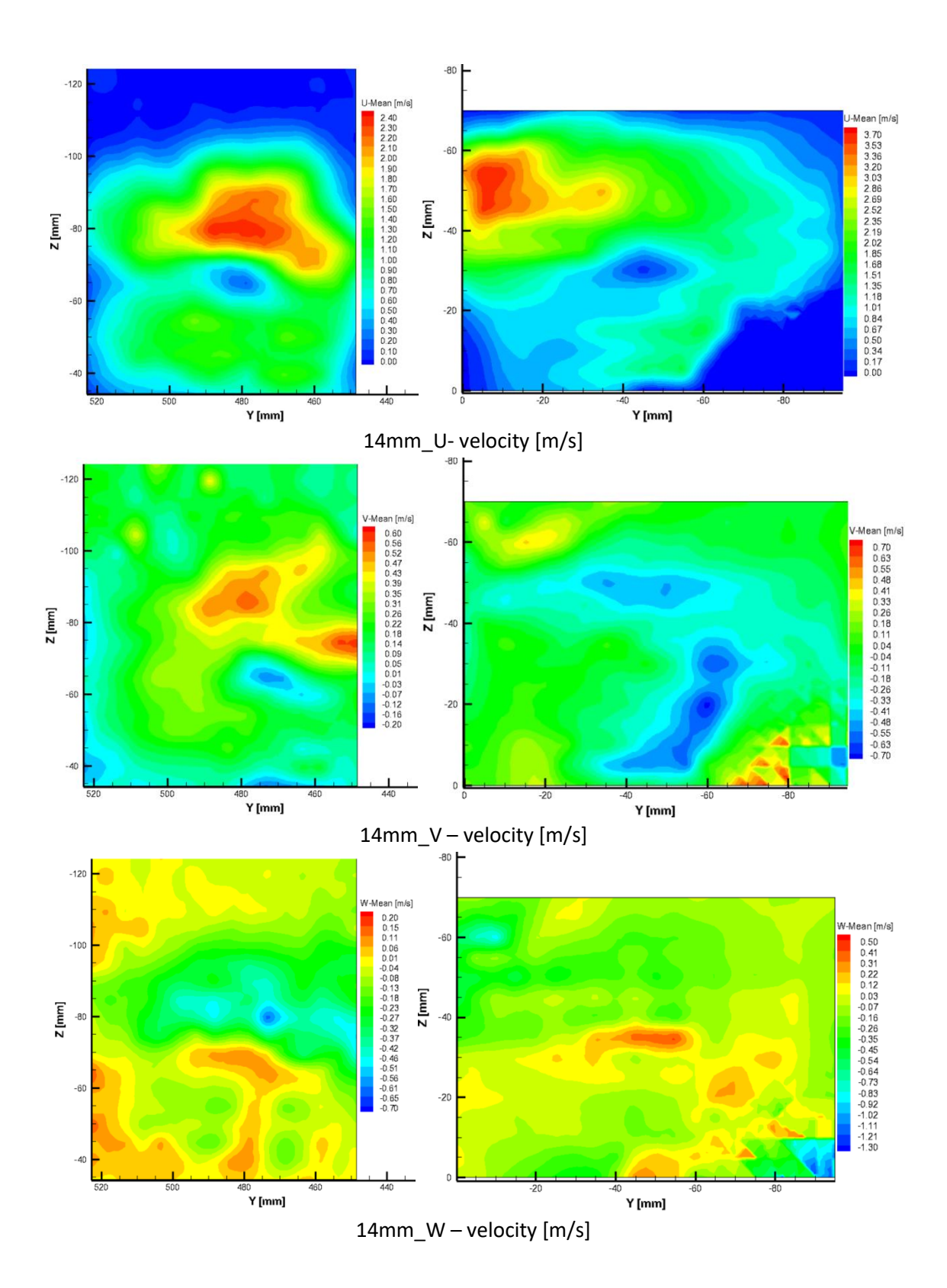
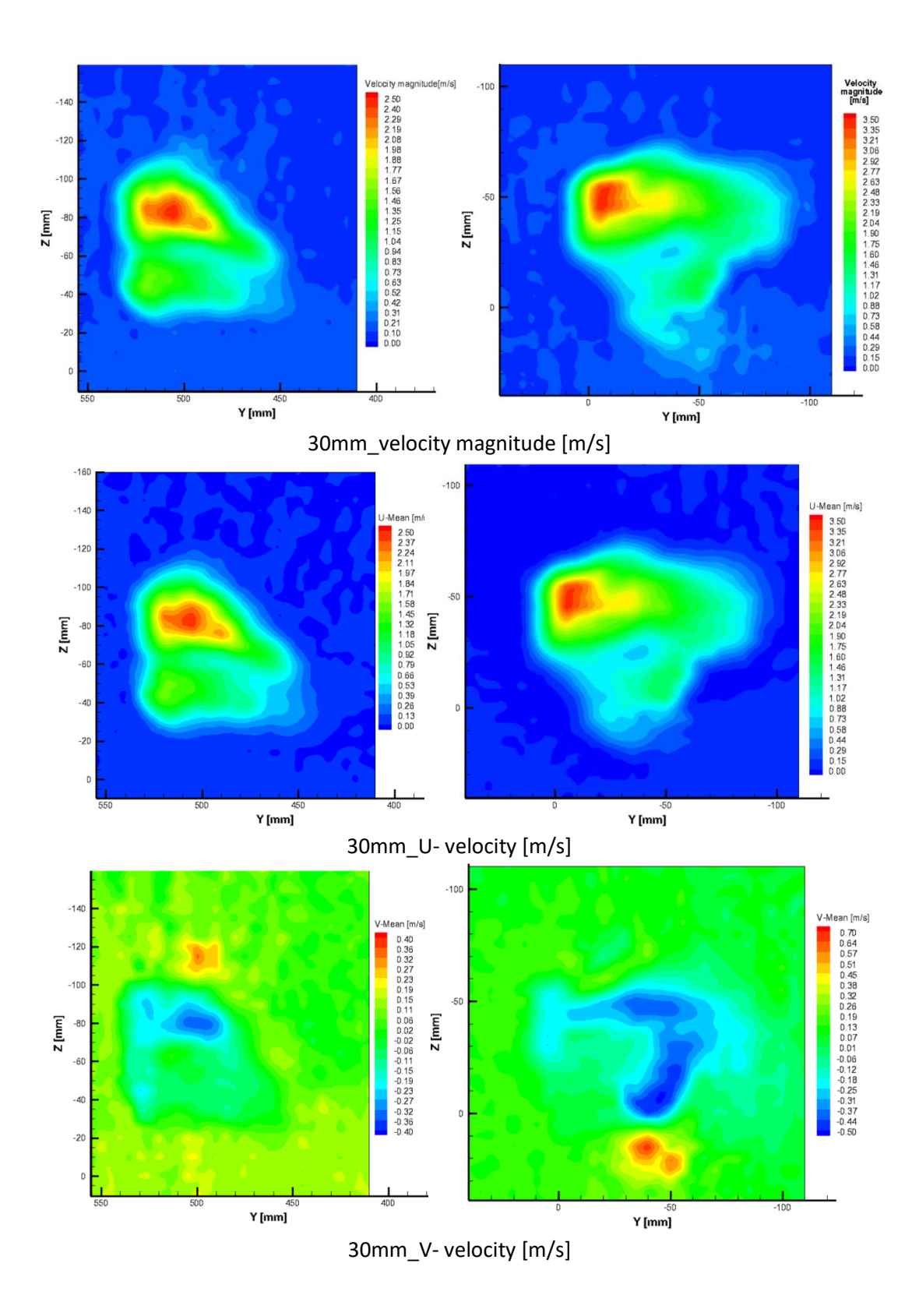


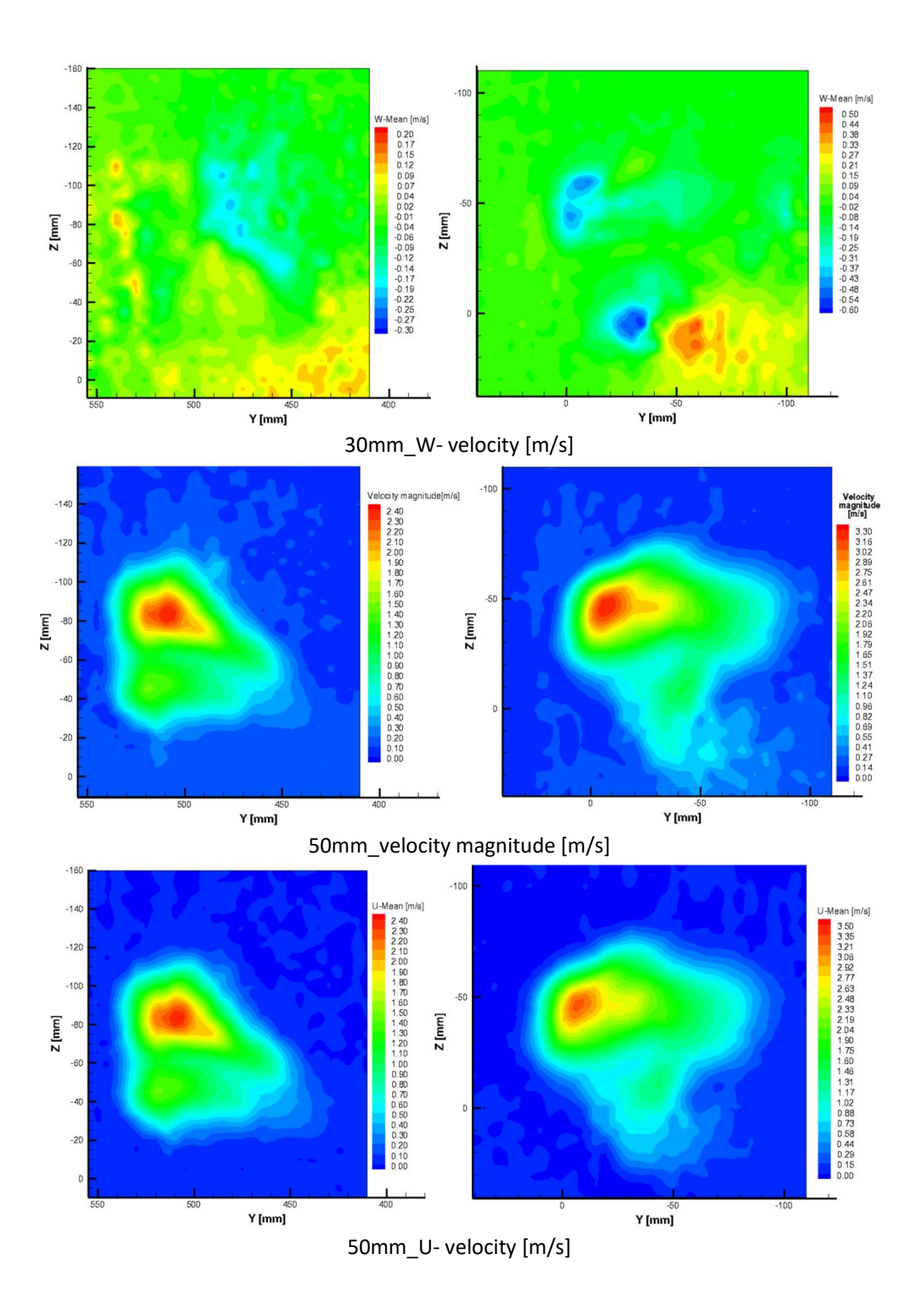
Figure 45. Used LDA 3D system

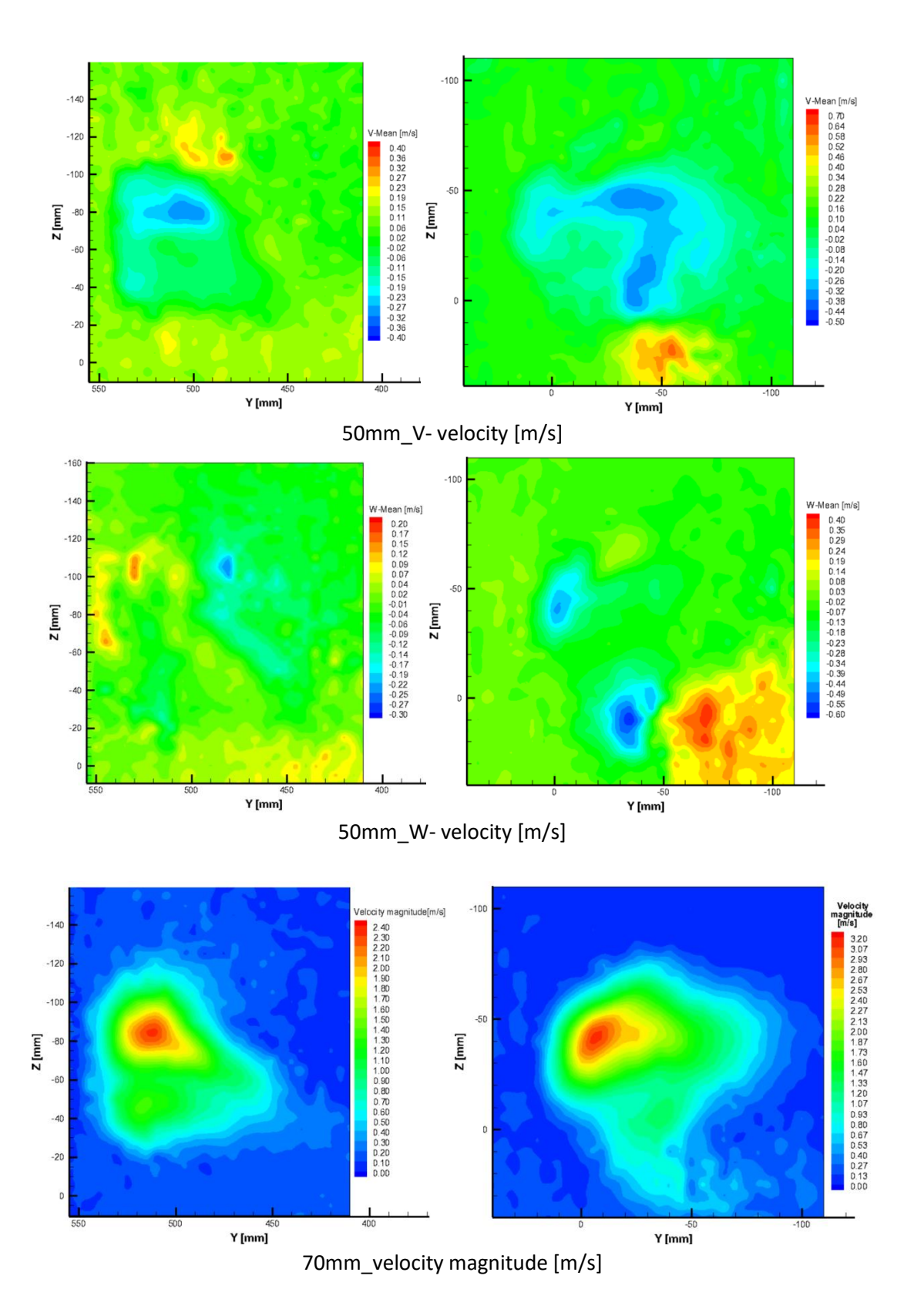
Results from LDA measurements- classical blowers.

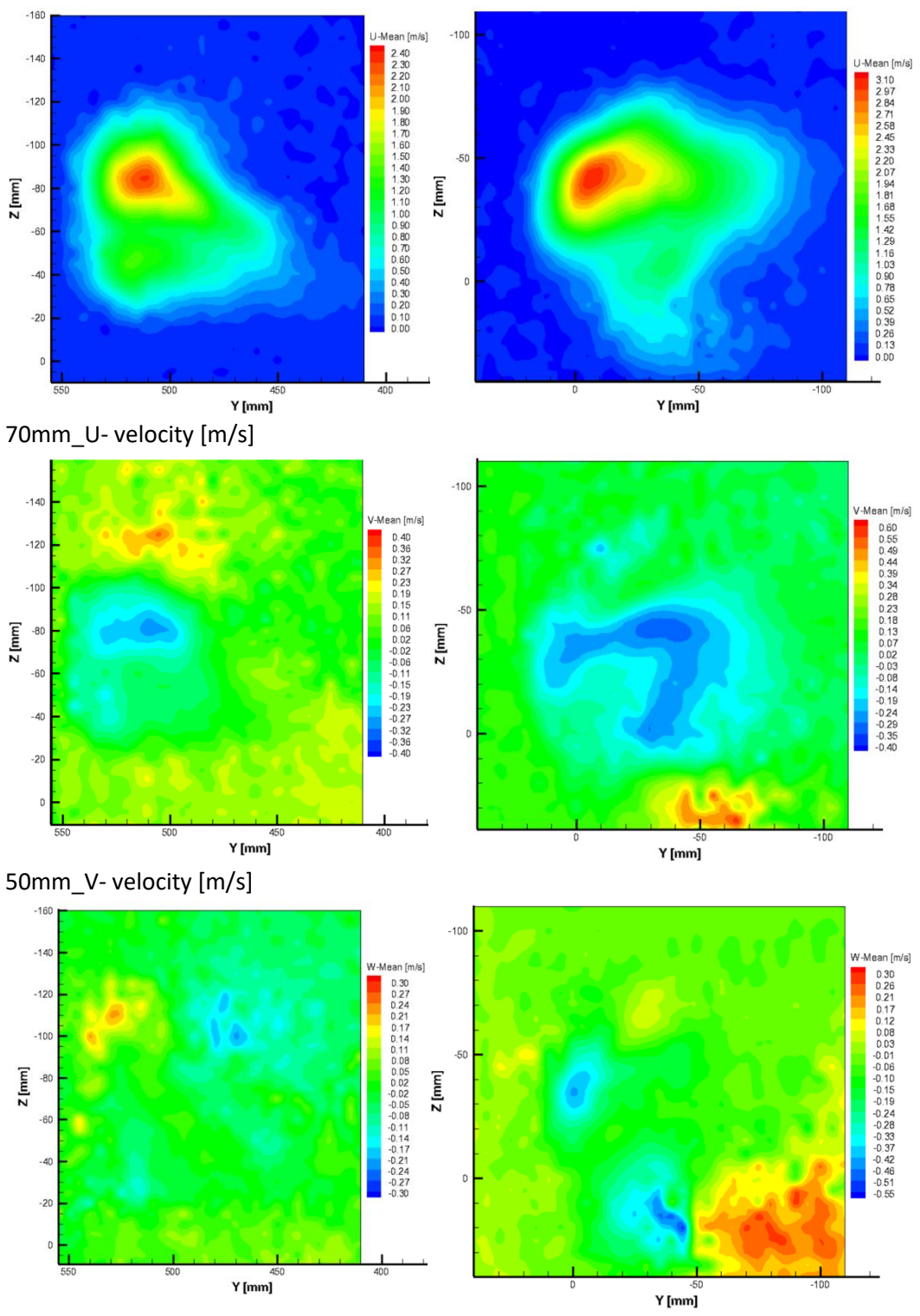




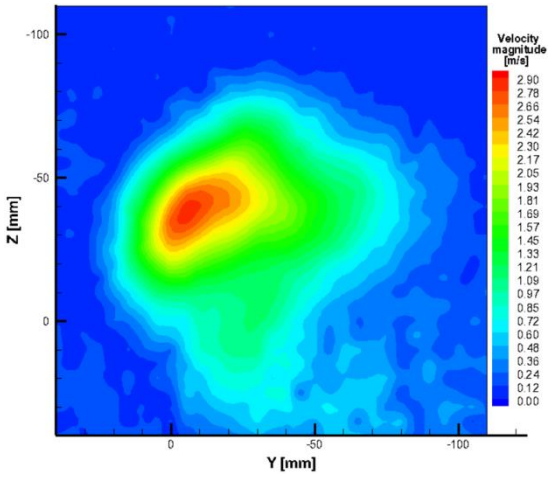




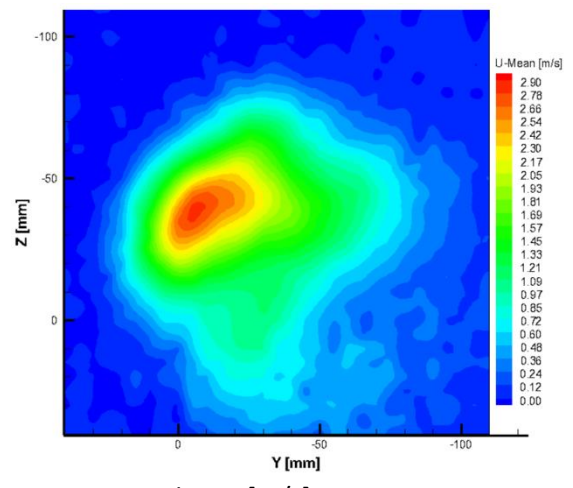




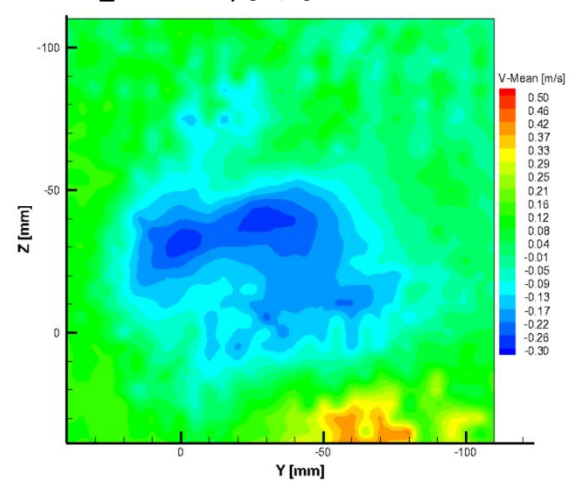
70mm\_W- velocity [m/s]



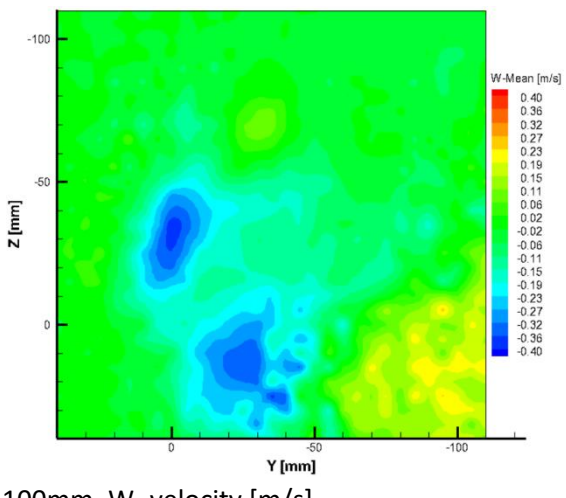
100mm\_velocity magnitude [m/s]



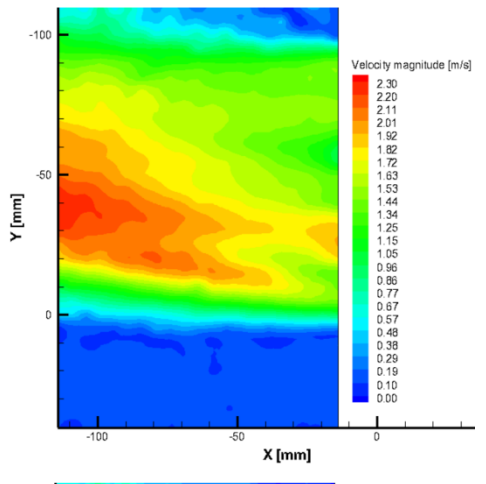
100mm\_U- velocity [m/s]

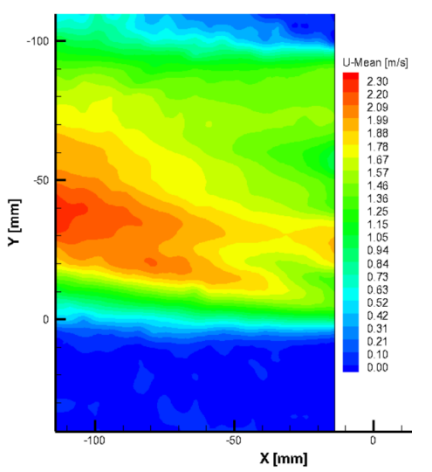


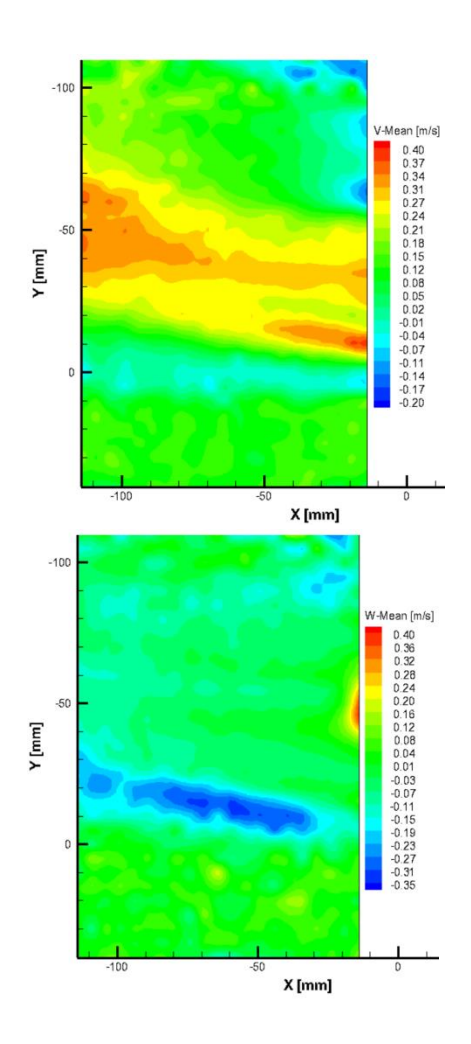
100mm\_V- velocity [m/s]

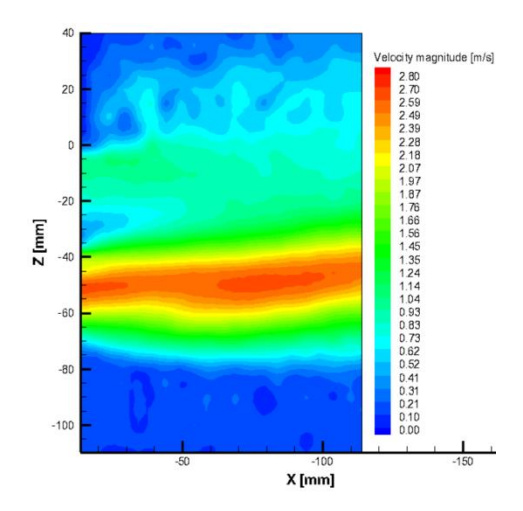


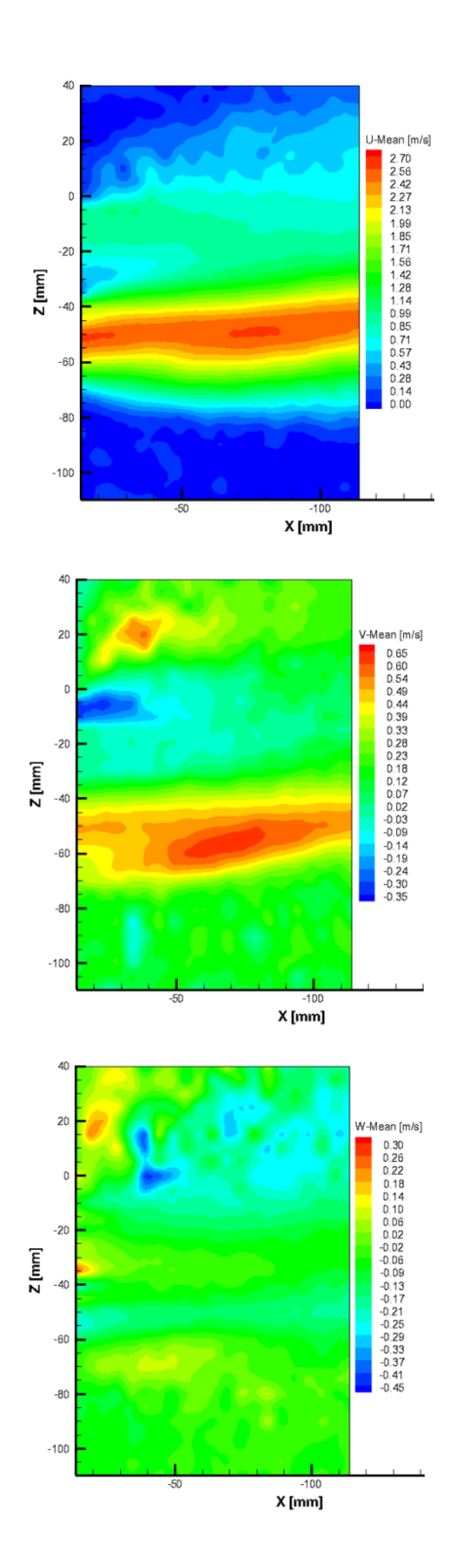
## 100mm\_W- velocity [m/s]











## 2. Numericam model tests

After validation of the reference numerical model in the previous study presented in [15], we decided to investigate the influence of the driver presence, over the thermal environment of a vehicle cabin. A second goal, the air flow direction imposed at the discharge over the global air velocity fields and the air flow patterns in the cabin car is investigated. We present in this article, results obtained for the air vent located on the dashboard at the driver's position (left side air vent) (see Figure 46).

Further we will call Case I – for the numerical simulations without virtual manikin; and Case II – numerical simulations with virtual manikin in the cabin. For each of these cases left grill airflow angle was modified on horizontal plane from 0° to 30°, with one step of 5° towards the interior cabin. In conclusion 14 numerical simulations were made for each case, each having a different angle.

To evaluate the effects of these different boundary conditions, 16 comparison points was considered (Figure 47), these points being positioned in at the head, chest, knee and foot levels in the place of the passengers.



Figure 46. Renault Megane dashboard, the considered air vent for the parametric variation of the angle of guiding vanes

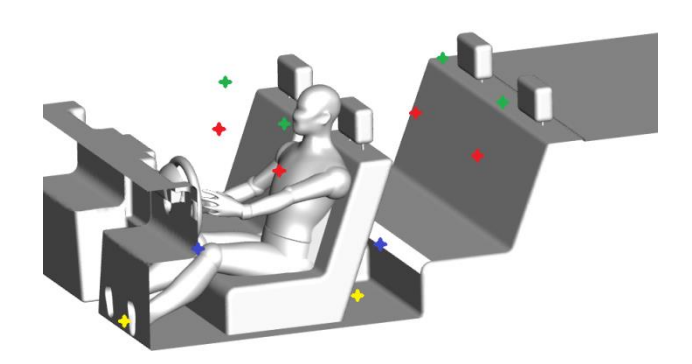


Figure 47 Considered measurement points at different levels: green – head; red – chest; blue – knee; yellow – foot;

Boundary conditions are like in the simulation case, except the temperatures values. We considered this study as isothermal; therefore the value of 23°C was imposed for the inlet air temperature, internal and external ambient temperature and on the cabin and manikin surfaces temperature. For the left side air vent, we modified the angle of the vertical guiding vanes in the horizontal plane from 0° to 30°, with a 5° step angle. Figure 48 and Figure 49 are presenting the distributions of the velocity magnitude and of the in-plane vectors for the median plane of the driver for both cases. One could observe that the global pattern of the flow inside the cabin is changing dramatically with the variation for only one air vent, and only in the horizontal plane.

Secondly the introduction of the human body, obstruct the air passing on the rear part of cabin, producing vortices in the neck and head zone of the driver .Starting with an angle of 20°, the velocity magnitude values in the drivers' chest region are higher than 1m/s. In the region of the face and chest for the rear left passenger the velocity magnitude displays values over 0.5m/s.The same observations could be done for the median plane of the passenger d).

Figure 50 and Figure 51. The flow pattern changes dramatically with the angle changing, while the presence of the manikin body diminishes air velocity in the rear part of the cabin.

Comparing the velocities found in rear part of the vehicle, high velocities was found in the rear right part of the car comparing with the rear left part. The causes are the inlet angle modification and the presence of the driver.

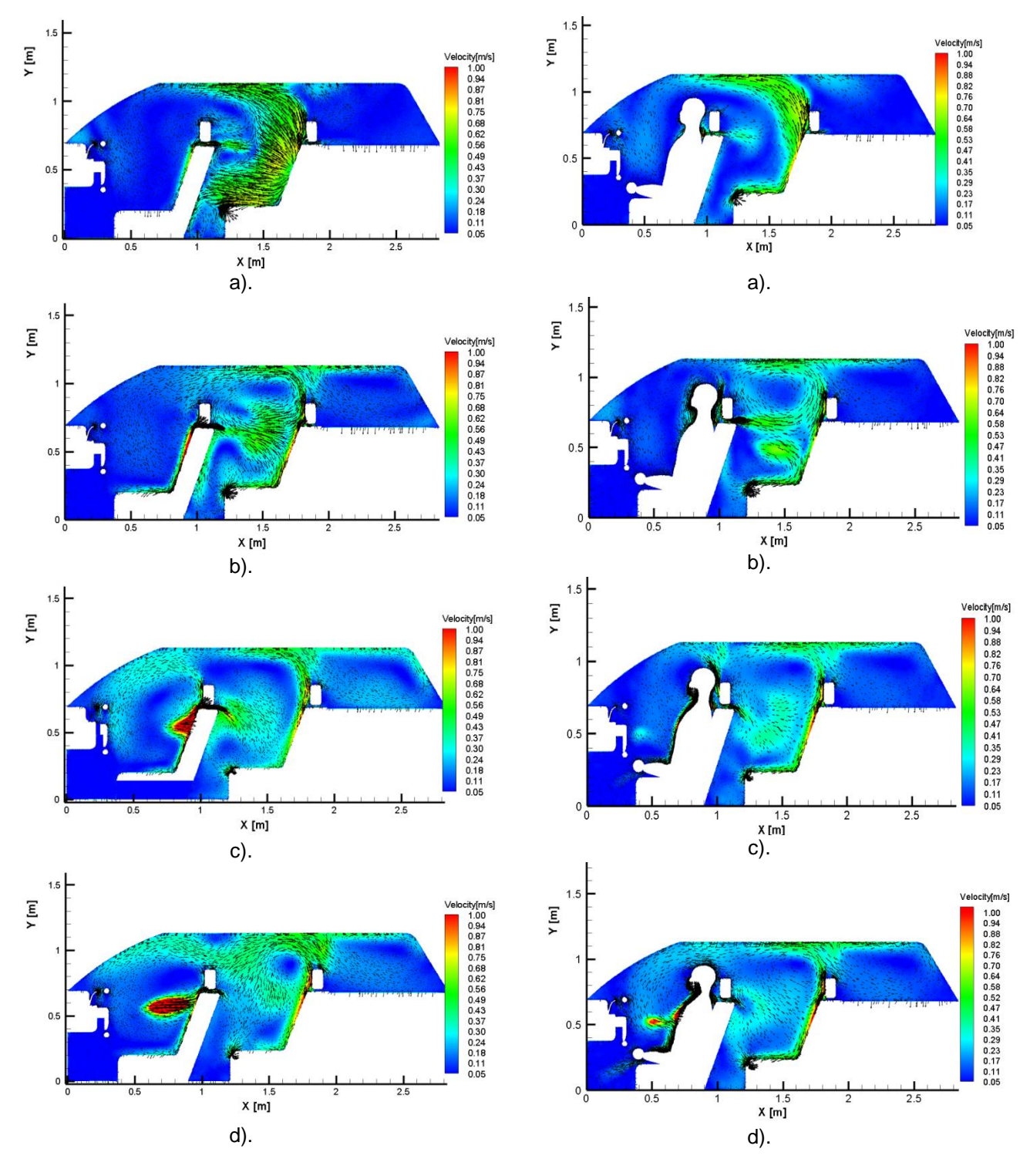


Figure48Distribution of the velocity magnitude and of the in plane vectors for the median plane of the driver: a). 0°; b). 10°; c) 20°; d) 30°, for Case I

Figure 49 Distribution of the velocity magnitude and of the in plane vectors for the median plane of the driver: a). 0°; b). 10°; c) 20°; d) 30°, for Case II

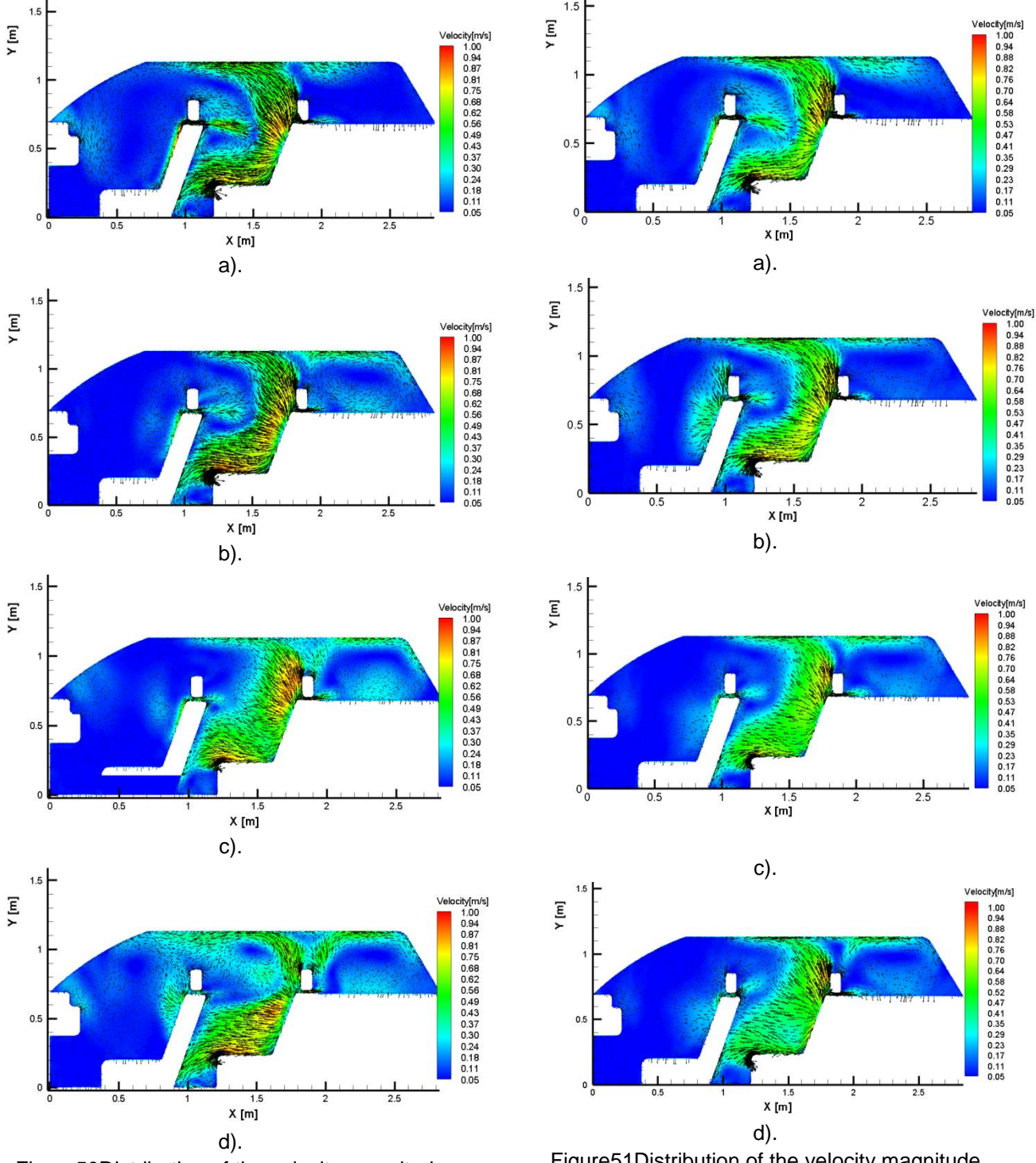


Figure 50 Distribution of the velocity magnitude and of the in plane vectors for the median plane of the passenger: a). 0°; b). 10°; c) 20°; d) 30°, for Case I

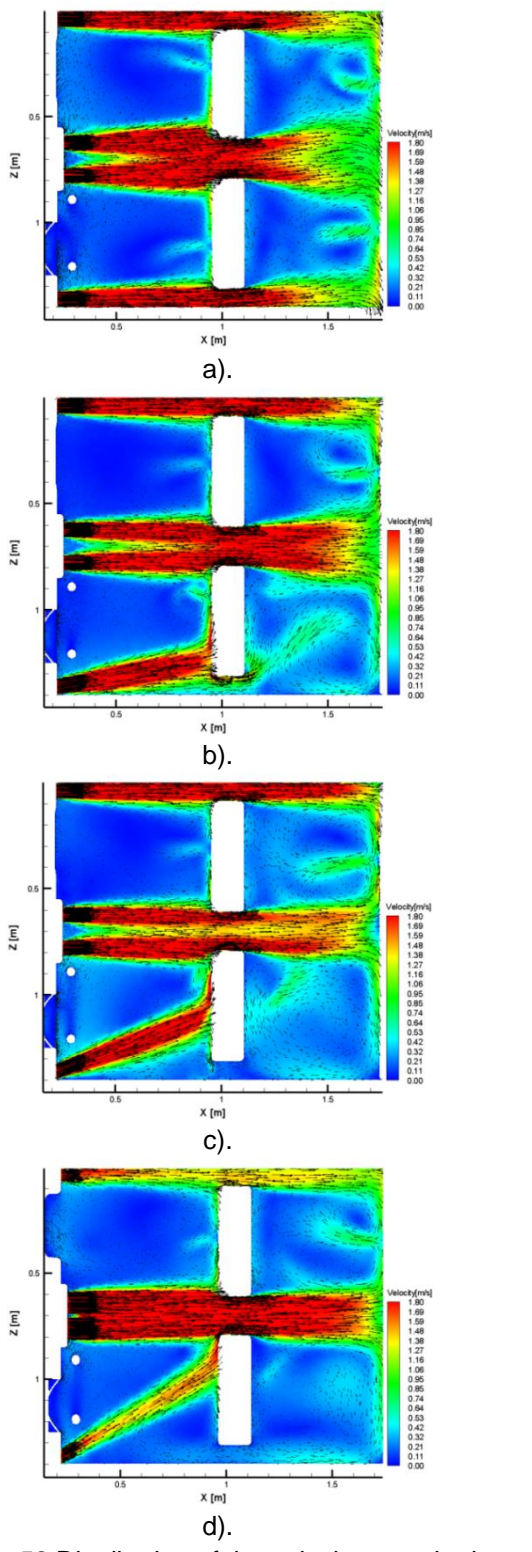


Figure 52 Distribution of the velocity magnitude and of the in plane vectors for the median plane of the passenger: a). 0°; b). 10°; c) 20°; d) 30°, for Case I

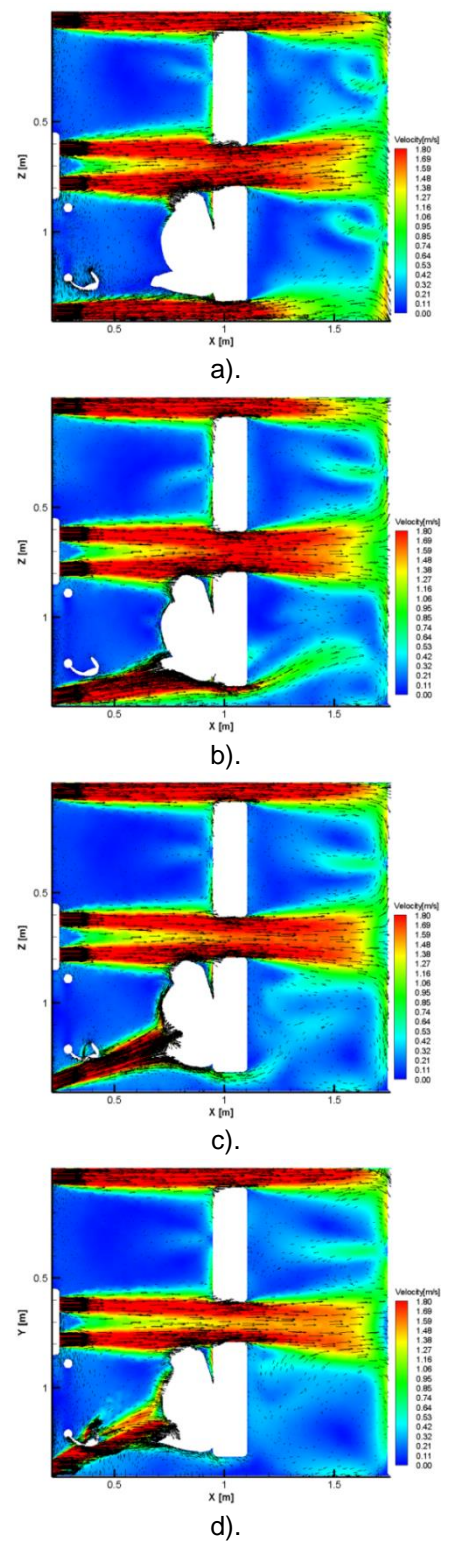


Figure 53 Distribution of the velocity magnitude and of the in plane vectors for the median plane of the passenger: a). 0°; b). 10°; c) 20°; d) 30°, for Case II

As a general observation, we note that the maximum values of the velocity magnitude are rather high compared to the limits of the PMVPPD models from the standards. Moreover, the locations of these maximum values are changing with the angle of the guiding vanes and the presence of the manikin geometry. However, given the high values recorded for the air velocities, the non-suitability of the PMV-PPD model is obvious, giving as a qualitative method of comparison in this case. These values are rather high at several locations when compared to the limits of the PMV-PPD model given in EN ISO 7730[16]. In the same time, the same study should be performed taking into account the thermal components, like the radiative transfer since the creation of recirculation regions with high velocities, resulting from the impinging of side flows on the windows could be benefic through the perspective of an enhanced heat transfer.

Table 3.PMV index comparison

Point/	0°		10°		20°		30°	
parameter	Case I	Case II	Case I	Case II	Case I	Case II	Case I	Case II
D. Head	-0.54	-0.54	-0.54	-1.00	-0.54	-0.54	-0.54	-0.58
P. Head	-0.54	-0.54	-0.54	-0.58	-0.65	-0.54	-0.71	-0.54
R.R. Head	-1.44	-1.45	-1.12	-1.15	-0.94	-0.93	-1.08	-0.85
R.L. Head	-1.50	-1.56	-1.53	-1.54	-1.59	-1.50	-1.23	-1.50
D. Chest	-0.54	-0.54	-0.58	-1.02	-0.80	-1.95	-2.08	-1.92
P. Chest	-0.54	-0.54	-0.74	-0.72	-0.72	-0.71	-0.60	-0.74
R.R. Chest	-1.53	-0.90	-1.19	-0.92	-0.94	-0.99	-1.07	-0.92
R.L. Chest	-1.49	-1.39	-1.56	-1.51	-1.47	-1.45	-1.61	-1.34
D. Knee	-0.54	-0.54	-0.54	-0.54	-0.54	-0.54	-0.54	-0.55
P. Knee	-0.63	-0.54	-0.54	-0.54	-0.54	-0.54	-0.54	-0.54
R.R. Knee	-0.98	-0.68	-0.77	-0.95	-1.02	-0.87	-0.83	-1.00
R.L. Knee	-1.44	-1.41	-1.46	-1.46	-1.45	-1.39	-1.48	-1.26
D. Foot	-0.54	-0.54	-0.54	-0.54	-0.54	-0.54	-0.54	-0.54
P. Foot	-0.54	-0.54	-0.54	-0.54	-0.54	-0.54	-0.54	-0.54
R.R. Foot	-0.58	-0.82	-0.72	-0.68	-0.72	-0.80	-0.54	-0.77
R.L. Foot	-0.80	-0.76	-0.80	-0.72	-0.54	-0.74	-0.54	-0.54

Knowing air velocity magnitude values from the numerical model and considering the metabolic rate value of 1 met and clothing insulation of 0.7 clo, the Predicted Mean Vote (PMV) and the Predicted Percentage of Dissatisfied (PPD) indexes were calculated. Tables Table 3 and Table 4 present values for the PMV and PPD indexes obtained at the right of each passenger place in the cabin for respectively the head, the chest, the knees and the feet. It appears from these tables that the most favorable position of the guiding vanes of the studied air vent is for an angle of 0°, knowing that most of PMV and PPD values fall in the acceptable range close to thermal neutrality. As the angle of the guiding vanes of the left air vent increases, values of PMV decreases showing an increased sensation of cooling.

This is translated by higher percentages of dissatisfied.

For the front passenger head we could not distinguish a clear trend for the variation of PMV/PPD values, most of them indicating much higher values for the velocity magnitude of air. As for the head region located at the position of the two rear passengers, all values of PMV fall between slightly cool and cool range.

From the Table 3 it appear that the PMV values have the tendency to a more comfortable state when the manikin in present than without manikin. Table 4 shows that the percentage of dissatisfied is smaller for the second case at 0° and 30°, with de high difference of 30,73% for R.R. Chest for 0°; and 14,33% for R.L. Chest. These differences are due to the manikin hand which intersects the flow from the left grill.

Table 4.PPD [%] index comparison

Point/	0°		10°		20°		30°	
parameter	Case I	Case II						
D. Head	11.23	11.23	11.24	26.16	11.23	11.23	11.23	11.99
P. Head	11.23	11.23	11.23	11.99	13.81	11.23	15.55	11.23
R.R. Head	48.05	48.51	31.45	32.83	23.75	23.25	29.94	20.36
R.L. Head	51.16	54.27	52.81	53.01	55.98	51.03	36.77	50.99
D. Chest	11.23	11.23	12.18	26.94	18.59	74.45	80.41	73.40
P. Chest	11.23	11.23	16.49	15.84	15.93	15.65	12.57	16.68
R.R. Chest	52.81	22.08	34.82	22.92	23.75	25.69	29.21	22.92
R.L. Chest	50.73	45.04	54.38	51.37	49.42	48.60	57.06	42.73
D. Knee	11.23	11.23	11.23	11.23	11.23	11.23	11.23	11.32
P. Knee	13.33	11.23	11.23	11.23	11.23	11.23	11.23	11.23
R.R. Knee	25.37	14.90	17.68	24.16	26.94	20.93	19.48	26.16
R.L. Knee	48.05	46.19	48.97	48.97	48.51	45.39	49.86	38.22
D. Foot	11.23	11.23	11.23	11.23	11.23	11.23	11.23	11.23
P. Foot	11.23	11.23	11.23	11.23	11.23	11.23	11.23	11.23
R.R. Foot	11.99	19.39	15.84	14.90	15.84	18.59	11.23	17.68
R.L. Foot	18.59	17.32	18.59	15.84	11.23	16.77	11.23	11.23

## **Bibliography**

- 1. Adrian, R.J., *Laser Velocimetry*, in *Fluid Mechanics Measurements*, R.J. Goldstein, Editor. 1983, Springer-Verlag. p. 155-240.
- 2. Calluaud, D. and L. David, Stereoscopic particle image velocimetry measurements of the flow around a surface-mounted block. Experiments in Fluids, 2004. 36(1): p. 53-61.
- 3. Nastase, I., *Analyse des jets lobés en vue de leur intégration dans les Unités Terminales de Diffusion d'air.* 2007, Université de La Rochelle: Ph.D. Thesis.
- 4. White, A.D. and J.D. Rigden, *Continuous Gas Maser Operation in the Visible*, v. Proc IRE, Editor. 1962. p. 1697.
- 5. Yeh, Y. and Z.H. Cummins, *Localized Fluid Flow Measurements with an He-Ne Laser Spectrometer*. Applied Physics Letters, 1964. 4(10).
- 6. Foreman, J.W., E.W. George, and R.D. Lewis, *Measurement of Localized Flow Velocities in Gases with a Laser Doppler Flowmeter.* Applied Physics Letters, 1965. 7(5).
- 7. Jr., R.C.W., R.D. Lewis, and H.J. Watson, *Instruments for Motion Measurement Using Laser Doppler Heterodyning Techniques*. ISA Trans, 1969. 8: p. 20-28.
- 8. Bruun, H.H., *Hot-Wire Anemometry Principles and signal processing* ed. O.S. Publication. 1995.
- 9. Meslem, A., Contribution à l'étude du couplage thermique entre un jet et un local climatisé. 1997, INSA Lyon.
- 10. Nilsson, H., et al. *Equivalent temperature and thermal sensation Comparison with subjective responses.* in *Comfort in the automotive industry- Recent development and achievements.* 1997. Bologna, Italy.
- 11. Bohm, M., et al., *Development of standard test methods for evaluation of thermal climate in vehicles*, in *Final Report on Project SMT4-CT95-2017*. 1999, Swedish Institute of Agricultural Engineering.
- 12. Nilsson, H.O., *Thermal comfort evaluation with virtual manikin methods.* Building and Environment, 2007. 42(12): p. 4000-4005.
- 13. ISO, Ergonomics of the thermal environment Evaluation of thermal environments in vehicles Part 2: Determination of equivalent temperature in ISO 14505-2:2006. 2006.
- 14. Jaramillo, J.E., et al., *Numerical study of plane and round impinging jets using RANS models*. Numer. Heat Transfer Part B 2008. 54: p. 213-237.
- 15. Chen, Q.Y., Z. Zhang, and W. Zuo. *Computational fluid dynamics for indoor environment modeling: past, present and future.* in *XXV UIT National Heat Transfer Conference.* 2007. Trieste, Italy.
- 16. Zhang, Z., J.Z. Zhai, and Q. Chen. *Evaluation of various CFD models in predicting room airflow and turbulence*. in *ROOMVENT*. 2007. Helsinki, Finland.